ASN NEURO RESEARCH ARTICLE

ASN NEURO 1(4):art:e00018.doi:10.1042/AN20090038

Targeted ablation and reorganization of the principal preplate neurons and their neuroblasts identified by golli promoter transgene expression in the neocortex of mice

Yuan-Yun Xie[1], Erin Jacobs and Robin Fisher[2]

Developmental and Molecular Neuroscience Group, Mental Retardation Research Center, Neuropsychiatric Institute, School of Medicine, The University of California at Los Angeles, Los Angeles, CA 90095, U.S.A.

Cite this article as: Xie Y-Y, Jacobs E and Fisher R (2009) Targeted ablation and reorganization of the principal preplate neurons and their neuroblasts identified by golli promoter transgene expression in the neocortex of mice. ASN NEURO 1(4):art:e00018.doi:10.1042/AN20090038

ABSTRACT

The present study delineates the cellular responses of dorsal pallium to targeted genetic ablation of the principal preplate neurons of the neocortex. Ganciclovir treatment during prenatal development (E11–E13; where E is embryonic day) of mice selectively killed cells with shared S-phase vulnerability and targeted expression of a GPT [golli promoter transgene, linked to HSV-TK (herpes simplex virus-thymidine kinase), τ-eGFP (τ-enhanced green fluorescent protein) and lacZ (lacZ galactosidase) reporters] localized in preplate neurons. Morphogenetic fates of attacked neurons and neuroblasts, and their successors, were assessed by multiple labelling in time-series comparisons between ablated (HSV-TK$^{+/0}$) and control (HSV-TK$^{0/0}$) littermates. During ablation generation, neocortical growth was suppressed, and compensatory reorganization of non-GPT ventricular zone progenitors of dorsal pallium produced replacements for killed GPT neuroblasts. Replacement and surviving GPT neuroblasts then produced replacements for killed GPT neurons. Near-normal restoration of their complement delayed the settlement of GPT neurons into the reconstituted preplate, which curtailed the outgrowth of pioneer corticofugal axons. Based on this evidence, we conclude that specific cell killing in ablated mice can eliminate a major fraction of GPT neurons, with insignificant bystander killing. Also, replacement GPT neurons in ablated mice originate exclusively by proliferation from intermediate progenitor GPT neuroblasts, whose complement is maintained by non-GPT progenitors for inductive regulation of the total complement of GPT neurons. Finally, GPT neurons in both normal and ablated mice meet all morphogenetic criteria, including the 'outside-in' vertical gradient of settlement, presently used to identify principal preplate neurons. In ablated mice, delayed organization of these neurons desynchronizes and isolates developing neocortex from the rest of the brain, and permanently impairs its connectivity.

Key words: morphogenesis, neocortex, neuron, plasticity, preplate, progenitor.

INTRODUCTION

Mammalian neocortex assembles in three developmental stages that reflect the successive fates of neurons generated by the proliferative zones of the dorsal pallium (Marin-Padilla, 1971; Rakic, 1988). Preplate neocortex forms first from the earliest-generated neurons, which are destined to persist in the mature subplate (Bayer and Altman, 1990; Verney and Derer, 1995; Reep, 2000; Robertson et al., 2000). Primitive neocortex forms next as the true cortical plate is

[1]Present address: Centre for Molecular Medicine and Therapeutics, Department of Medical Genetics, University of British Columbia, Vancouver, B.C., Canada, V5Z 4H4

[2]To whom correspondence should be addressed (email rfisher@mednet.ucla.edu).

Abbreviations: BrdU, bromodeoxyuridine; CSF, cerebrospinal fluid; DAB, 3,3′-diaminobenzidine; E, embryonic day; τ-eGFP, τ-enhanced green fluorescent protein; GPT, golli promoter transgene; *h*, counted profile thickness; HSV-TK, herpes simplex virus-thymidine kinase; i.p., intraperitoneal; lacZ, lacZ galactosidase; MAT, metaphase, anaphase and telophase; MBP, myelin basic protein; n.a., numerical aperture; P, postnatal day; T_s, section thickness; TUNEL, terminal deoxynucleotidyltransferase-mediated dUTP nick-end labelling; X-gal, 5-bromo-4-chloro-3-indolyl-β-D-galactoside.

established by later-generated neurons, which are destined to persist as infragranular pyramidal cells (Valverde et al., 1995; Adams et al., 1997; Meyer and Wahle, 1999; Super and Uylings, 2001; Zecevic and Rakic, 2001). Mature neocortex forms finally as the cortical plate is penetrated and blanketed by the last-generated neurons, which are destined to persist as granular and supragranular pyramidal cells. Throughout this sequence, a small complement of non-pyramidal neurons (<10% of total) generated at the margins of the dorsal pallium migrate tangentially into the developing neocortex (Del Rio et al., 1997; Meyer and Wahle, 1999; Hevner and Zecevic, 2006).

The principal preplate neurons show radial migration like the predominant cortical plate neurons. They are proliferated by progenitor cells, and many, if not all, of the more deeply settled preplate neurons emit corticofugal pioneer axons before cortical plate neurons. Unlike cortical plate neurons, they have an 'outside-in' neurogenetic gradient of vertical settlement and, for the most part, shorter periods of survival. They serve primarily as a transient mould for neocortical morphogenesis by support of radial migration, laminar framing and guidance of afferent ingrowth (Ghosh and Shatz, 1993; Allendoerfer and Shatz, 1994; McConnell et al., 1994; Molnar and Blakemore, 1995; Ogawa et al., 1995; Del Rio et al., 1997; Molnar et al., 1998; Super et al., 1998; Super and Uylings, 2001; Sarnat and Flores-Sarnat, 2002). However, their full developmental role remains uncertain owing to limited success in their identification and experimental elimination. Most of the molecular markers of these cells occur in multiple brain sites and have insufficient anatomical isolation for decisive ablation studies (Hevner et al., 2003). Furthermore, the normal expression of these markers may not regulate naturally occurring mechanisms of apoptosis.

Fortunately, the transgene of the proximal golli promoter of the MBP (myelin basic protein) gene is a promising molecular marker for such analyses because of its early and restricted expression in cerebral cortex, olfactory bulb and sensory ganglia in mice. It can be used to drive expression of various reporters, including HSV-TK (herpes simplex virus-thymidine kinase), which putatively identify the principal preplate neurons and their neuroblasts [collectively referred to as GPT (golli promoter transgene) cells for ease of expression] (Landry et al., 1998; Xie et al., 2002; Jacobs et al., 2007). HSV-TK can convert the prodrug ganciclovir into toxic nucleotide analogues that disrupt DNA synthesis in genetically targeted GPT progenitors. This initiates apoptosis in their daughter GPT cells (neurons and/or neuroblasts), which complete mitotic division after shared S-phase vulnerability (Moolten, 1986). Such treatments produce characteristic global defects of neocortical lamination in transgenic mice (Xie et al., 2002). In the present study, we focus on the early cellular aspects of this phenotype to test the hypothesis that a permanent, catastrophic extermination of GPT neurons accounts for these ablations. The origins, fates and organizations of GPT cells are compared in time-series between littermate control and genetically targeted mice with equivalent exposures to ganciclovir.

MATERIALS AND METHODS

Most of the methods used here have been described fully previously (Landry et al., 1998; Xie et al., 2002; Jacobs et al., 2007). New observations were obtained from 305 mice (160 HSV-TK$^{+/0}$ experimental mice; 145 HSV-TK$^{0/0}$ control mice) randomly selected from 46 timed pregnancies [day of mating=E0.5 (where E is embryonic day); day of birth=P1 (where P is postnatal day)] treated to produce large ablations, 107 mice (56 HSV-TK$^{+/0}$; 51 HSV-TK$^{0/0}$) randomly selected from 24 timed pregnancies treated to produce smaller ablations, and normative reference materials. Data from males and females were equivalent and pooled. Mice were housed in the UCLA School of Medicine vivarium, and procedures were conducted according to the NIH (National Institutes of Health) *Guide for the Care and Use of Laboratory Animals*.

Generation and ablation of transgenic mice

Establishment and histological identification of genotypes

Transgenic genotypes were produced using the proximal GPT for the *MBP* gene to drive expression of linked, non-native reporter transgenes for HSV-TK, τ-eGFP (τ-enhanced green fluorescent protein) and/or lacZ (lacZ galactosidase) (Landry et al., 1998; Xie et al., 2002; Jacobs et al., 2007). The GPT element inserted into all mice was a fragment containing 1.1 kb upstream of the golli transcription start site plus 0.2 kb downstream into the first exon of the *MBP* gene. Two transgenic lines were studied. Double transgenics were generated by crossing hemizygous HSV-TK and homozygous lacZ mice to produce HSV-TK$^{+/0}$/lacZ$^{+/+}$ (experimental) and HSV-TK$^{0/0}$/lacZ$^{+/+}$ (control) mice. Triple transgenics were generated by crossing mice from the double genotype with homozygous τ-eGFP mice to produce HSV-TK$^{+/0}$/τ-eGFP$^{+/0}$/lacZ$^{+/0}$ (experimental) and HSV-TK$^{0/0}$/τ-eGFP$^{+/0}$/lacZ$^{+/0}$ (control) mice.

Cross-validation of genotypes by PCR

The GPT/HSV-TK transgene was identified in founder breeders and all experimental mice by PCR using the MGTB sense primer 5′-CTGAGCTTCACGACCCCGGAACATAGT-3′ (within GPT) and the HSV-TK3P antisense primer 3′-GTCATGCTGCCCATAAGGTATCGCG-5′. The GPT/lacZ transgene was identified in all mice using the MGTB sense primer and the β-galactosidase antisense primer 3′-CTCATCCGCCACATATCCTGATCTTCC-5′. For PCR amplification, a 25 µl reaction mixture was assembled containing 200 ng of genomic DNA, 10 pmol of primer, 4 mM $MgCl_2$, 0.2 mM dNTPs, PCR buffer and 1.25 units of Taq DNA polymerase (Invitrogen). After denaturation, PCR products were analysed on a 1% agarose TAE gel. As described previously (Landry et al., 1998; Xie et al., 2002; Jacobs et al., 2007), the HSV-TK reporter in experimental mice was 0.6 kb and the lacZ β-galactosidase reporter in all mice was 1.1 kb.

Southern blots showed the τ-eGFP reporter as 1.4 kb and 0.82 kb GFP fragments in all triple transgenic mice.

Ganciclovir treatments

Ganciclovir (Cytovene-IV™, Roche Laboratories) was made up to 0.25 mg/ml in a water vehicle. For the main treatment group with the largest ablations, pregnant dams received two i.p. (intraperitoneal) injections of ganciclovir (20 μg/g of body weight) on E11 and E12 (four injections at 10–12 h intervals) (Xie et al., 2002). For smaller ablations, useful to determine the effects of multiple doses and timing of ganciclovir administrations, pregnant dams received ganciclovir treatments on the following schedules: three injections on E11–E12, two injections on E11, E12, E13, E14, E15 or E17, one injection on E11 and one injection on E12, and one injection on E11. These age groups were selected due to the positive expression of HSV-TK in ventricular zone progenitors shown on E11–E15. Unablated experimental mice receiving vehicle instead of ganciclovir on E11–E12 had no neocortical damage. All mice were alive at delivery as indicated by spontaneous movement and/or the absence of histological signs of fetal resorption or extended anoxia.

Histological preparations

Tissue processing

Pregnant dams anaesthetized with halothane were killed by cervical dislocation to obtain fetal tissue on E11–E16 and E18. Fetuses were delivered, brains dissected and tissues immersed in 0.9% NaCl and 4% (w/v) paraformaldehyde in 0.1M PBS fixative. Postpartum mice anaesthetized with halothane were perfused transcardially with fixative to obtain tissue on P1 and P4. Tissues were immersion-fixed for 1 h (histochemistry) or 12 h (immunohistochemistry) at 4°C, cryoprotected in 30% (w/v) sucrose, frozen in OCT™, sectioned serially at 20 μm thickness (coronal or sagittal planes; all age groups included specimens in both cardinal planes), and mounted on subbed glass slides. For coronal series, the section interval was 200 μm along the rostrocaudal axis of forebrain.

Primary antibodies

HSV-TK was localized with polyclonal rabbit anti-HSV-TK serum [a gift from Dr WC Summers (Yale University School of Medicine, New Haven, CT, U.S.A.); 1:2000 dilution]. Directed against whole purified protein, this antiserum shows a major 45 kDa band with minor 40–43 kDa bands for HSV-TK in Western blot analysis (Bush et al., 1998). Label was detected in all mice with, and none without, the GPT/HSV-TK transgene, indicative of primary antiseral specificity (Figures 3C–3E). τ-eGFP was localized with a polyclonal rabbit anti-GFP serum (Chemicon, catalogue number AB3080; 1:1000 dilution) or a monoclonal mouse anti-GFP antibody (Clontech, catalogue number 632375; 1:1000 dilution), which show a single 27 kDa band for GFP in Western blot analysis (according to the manufacturer's instructions). Label was detected in all mice with, and none without, the GPT/τ-eGFP transgene, indicative of primary antibody specificities. BrdU (bromodeoxyuridine) was localized with a monoclonal mouse anti-BrdU antibody (Becton Dickinson, catalogue number 555627; 1:100 dilution), which shows BrdU incorporated into single-stranded DNA during the S-phase of the cell cycle (according to the manufacturer's instructions). Label was restricted to the progeny of cells that underwent the cell cycle and mitosis during the periods of BrdU exposure, indicative of primary antibody specificity.

HSV-TK immunohistochemistry

Sections from experimental and control mice in litters with or without ganciclovir treatment were obtained on E11 (a pre-ablation group from the earliest day of clear GPT expression in forebrain), E12, E13, E15 and E18. Only HSV-TK$^{+/0}$ experimental mice expressed this transgene, so unablated experimental HSV-TH$^{+/0}$ mice from dams treated with vehicle, but not ganciclovir, provided normative data. Mounted specimens were treated with 0.3% H_2O_2/methanol, blocked in normal rabbit serum, incubated in primary antiserum and labelled by biotinylated avidin–peroxidase methods using DAB (3,3′-diaminobenzidine) chromogen. Method specificity of labelling in GPT neurons and neuroblasts was affirmed by differential staining of 'experimental' compared with 'control' sections after omission of primary antiserum in each experimental case, with no apparent labelling in HSV-TK$^{0/0}$ control mice (Figures 3C–3E). For reporter cross-validation, sections were labelled for lacZ, then HSV-TK. Reporter co-localization was determined microscopically (brown cytoplasmic/nucleoplasmic HSV-TK label+blue cytoplasmic lacZ label; Figure 3A), with optical elimination of each label by a running continuous interference monochromator. Results were obtained from 53 cases (14 ablated experimental+15 unablated experimental+24 control mice; 13 litters).

τ-eGFP immunohistochemistry

For intrinsically generated eGFP, mounted specimens were coverslipped in Aquamount™ (Figures 12A–12F). Immunohistochemical methods improved label efficiency. Mounted specimens were quenched with 0.3% H_2O_2/methanol, blocked with BSA, incubated in primary antibodies and labelled by biotinylated avidin–peroxidase methods using DAB chromogen. Method specificity of labelling of GPT neurons was affirmed by omission of primary antibodies in 'control' sections from each case. For reporter cross-validation, sections were labelled for lacZ, then τ-eGFP. Reporter co-localization was determined microscopically (brown cytoplasmic τ-eGFP label+blue cytoplasmic lacZ label; Figure 3B), with optical elimination of each label. Results were obtained from E14–P4 mice. Single labels of τ-eGFP by intrinsic fluorescence and immunoperoxidase methods were compared in ten cases (six ablated+four control mice) with equivalent results. Another

17 cases (ten ablated+seven control mice) were tested for co-localization of HSV-TK, τ-eGFP and lacZ where serial sections were double-labelled for each reporter combination. Reference data from 12 immunoperoxidase cases (E12–P1) have been reported previously (Jacobs et al., 2007).

LacZ β-galactosidase histochemistry

Mounted sections were treated in 0.01% sodium deoxycholate, 0.02% Nonidet P40, 2 mM $MgCl_2$ and 0.1 M $NaHPO_4$ (pH 7.3), for 10 min at room temperature (22°C) then incubated in X-gal (5-bromo-4-chloro-3-indolyl-β-D-galactoside) labelling solution [2 mM $MgCl_2$, 5 mM $K_3Fe(CN)_6$, 5 mM $K_4Fe(CN)_6$ plus 0.1 M $NaHPO_4$ (pH 7.3), 0.01% sodium deoxycholate, 0.02% Nonidet P40 and 8 mg/ml X-gal] for 6–16 h at 37°C followed by a PBS stop-bath. Method specificity of labelling of GPT neurons was affirmed by omission of X-gal treatment in 'control' sections from each case. Labelled sections were used for co-localization experiments and counterstained with Neutral Red (Figures 4A–4F; 205 cases), good for photomacroscopy, or Harris haematoxylin (regressive method; 78 cases, E12–P4, three to five cases/age and genotype group), for improved recognition of degenerating cells, mitotic profiles and neocortical laminae.

TUNEL (terminal deoxynucleotidyltransferase-mediated dUTP nick-end labelling) *in situ* labelling

Apoptotic cells were identified by pyknosis in lacZ sections counterstained with haematoxylin and TUNEL in lacZ sections. Mounted specimens were labelled for lacZ, quenched in 0.3% H_2O_2/methanol, permeabilized by 0.1% Triton X-100, incubated in TUNEL reaction mixture for 1 h at 37°C (*In Situ* Cell Death Detection Kit, POD, Roche), followed by Convertor-POD reagent and peroxidase substrate with DAB chromogen. Method specificity of labelling of apoptotic cells was affirmed by omission of TUNEL reaction treatment in 'control' sections from each case. After labelling for lacZ, TUNEL co-localization in apoptotic GPT cells was determined microscopically in single sections (blue cytoplasmic lacZ label+brown cytoplasmic/nucleoplasmic TUNEL label) and cross-validated by optical elimination. Observations were obtained from 52 cases at E12–P4 (26 ablated+26 control mice, 15 litters, half tested for lacZ+pyknosis and half tested for lacZ+TUNEL).

BrdU immunohistochemistry

The ages of proliferation of GPT neurons from progenitors were determined by double-labelling with lacZ and BrdU. After BrdU injections, fetuses were allowed to survive for various periods to reveal settlement patterns of BrdU-labelled cells, with particular regard to 'birth-dated' G_0-phase neurons. On E12–E16, pregnant dams in the main ablation group (E11–E12 ganciclovir treatments) were given an i.p. injection of 100 μg of BrdU/g of body weight in PBS vehicle. E12-injected fetuses were harvested on E13 and E14 (24 and 48 h post-BrdU; 24–48 h post-ganciclovir). E13-injected fetuses were harvested on E15 and E16 (48 and 72 h post-BrdU; 72–96 h post-ganciclovir). E15-injected fetuses were harvested on E17 (48 h post-BrdU; 120 h post-ganciclovir). E16-injected fetuses were harvested on E18 (48 h post-BrdU; 144 h post-ganciclovir). Sections were labelled for lacZ then incubated in 2 M HCl for 30 min at 37°C, rinsed in 0.1 M sodium borate (pH 8.3), and incubated overnight in anti-BrdU antibody. Labelling of BrdU was obtained by biotinylated avidin–peroxidase methods using DAB chromogen. Method specificity of BrdU-labelling of GPT cells was affirmed by omission of anti-BrdU in 'control' sections from each case. Label co-localization was determined microscopically (blue cytoplasmic lacZ label+brown nucleoplasmic BrdU label; Figure 3F) and cross-validated by optical elimination. Overall, 54 cases (28 ablated+26 control mice, 17 litters) were examined.

Morphological analysis

Histological differences were assessed by comparisons between and within genotype, treatment and age groups. Observations were obtained by light microscopy with brightfield transmission, differential interference contrast transmission and epifluorescent illumination (Zeiss Ultraphot IIIB and Leica DMRXA microscopes). Data were recorded by analogue film and digital photography as well as camera lucida mapping. Trends observed by qualitative methods were pursued by quantitative measurements, mainly density indices of specifically labelled cells, to assess statistical reliability of differences between groups. Neocortical development was bilaterally symmetrical in all groups, so data were obtained from a randomly selected hemisphere from each case. Neocortex has a lateral-to-medial horizontal neurogenetic gradient reflected in the vertical extent and density of GPT neurons, so sampling sites were selected from its flat-mapped centre where measurements approximated averages from lateral and medial limits. Under certain conditions, ablated mice had focal neocortical scars. Sampling sites were selected in the unscarred dorsal pallium to assure homologous locations between groups that were well-lateral to the scarred regions.

A comprehensive density index of GPT neurons was derived from nine measurements/case of lacZ-positive cells in Neutral Red-counterstained neocortex of experimental and control mice. Age groups were E12–E16, E18, P1 and P4 (66 ablated mice+61 control mice, 29 litters, five to ten mice/age and genotype). In medial, middle and lateral sampling sites from a central and two adjacent sections, non-pyknotic lacZ cells with nuclear profiles were detected by light microscopy [20 × objective, n.a. (numerical aperture) 0.6, 200 × total magnification] and counted in 2.4×10^{-1} mm^2 areas between superficial pial and deep lateral ventricular borders.

Statistical differences between groups were robust, so equivalent decisions were usually obtained from more efficient standard density indices. For example, comparable

densities of GPT neurons were derived from one measurement/case of lacZ-positive cells in haematoxylin-counterstained neocortex using the age groups described above (40 ablated mice+38 control mice, 19 litters, three to five mice/age and genotype). In sampling sites from a central section, non-pyknotic lacZ cells with nuclear profiles were detected by light microscopy ($25\times$ objective, n.a. 0.65, $625\times$ total magnification) and counted throughout a viewing field centred on the intermediate/mantle zone junction (305 μm diameter, 7.3×10^{-2} mm^2). Measurements from each case were corrected for the percentage of the viewing field occupied by tissue, converted into volume densities and extrapolated to labelled neurons/mm^3 of neocortex. These values, normalized by tissue unit, were grouped by age and genotype, averaged, and compared statistically, mainly by a one-way Student's *t* test with a fixed $P_\alpha<0.05$ as the criterion of reliable differences between groups. These standard density estimates were also used to measure apoptotic and BrdU-labelled neurons.

Finally, in central sections from E12–E14 mice counterstained with haematoxylin (15 ablated mice+13 control mice, three to five mice/age and genotype), mitotic cells with recognizable cleavage planes (as signified by chromosomal orientation, nuclear division and/or cytoplasmic division) and locations <25 μm from the ventricular surface were detected by light microscopy and counted along 500 μm of the ventricular lumen of the dorsal pallium ($63\times$ oil objective, n.a. 1.4, $1260\times$ total magnification). Among these cells, MAT [M (metaphase), A (anaphase) and T (telophase)] mitotic profiles were categorized as horizontal (cleavage planes $<45°$ from a line parallel to the apical cell surface) or vertical (cleavage planes $<45°$ from a line perpendicular to the apical cell surface). Within each group, MAT profiles yielded comparable percentages of horizontal and vertical cells, which allowed the data to be pooled across these mitotic phases into two comprehensive categories despite metaplate rocking during metaphase (Haydar et al., 2003). Measurements from each case were converted into linear densities, extrapolated to cells/mm of ventricular surface length for normalization and grouped for statistical analyses.

For all of these measurements, Abercrombie's correction $[T_s/(T_s+h)]$; where T_s is section thickness and h is counted profile thickness] was applied to reduce the bias of profile counts from serial tissue sections (Guillery, 2002). Both terms of the correction factor were nearly constant across the age and treatment groups ($T_s=20$ μm; $h=5$ μm). Thus the 0.80 correction ratio was a transformation that increased the accuracy of the description, with no effect on the validity of conclusions based on the raw data.

RESULTS

Ablation studies customarily begin with a survey of the extirpated tissue. The genetically targeted ablation used in the present study was unusual because it identified the specifically killed tissue elements as GPT cells, whose survivors showed in turn a high degree of reconstitution and replacement in reaction to the loss of their predecessors within a defective neocortical phenotype. Our analysis first compared control and ablated mice to assess the structural organization of excess dying GPT cells and to delineate their place within the scheme of reorganization of viable GPT cells, which would have been their normal fate without ganciclovir treatment.

Excess dying GPT cells and a defective neocortical phenotype (Xie et al., 2002) were reliably associated with genotype, ganciclovir treatment and age at ganciclovir treatment ($P_\alpha<0.05$). HSV-TK$^{0/+}$ experimental mice, but not HSV-TH$^{0/0}$ control mice with identical exposure to ganciclovir, had the defective phenotype. Ganciclovir-treated experimental mice, but not untreated (i.e. vehicle-injected) experimental mice, had the defective phenotype. Unablated experimental mice had the normal neocortical phenotype of control mice. Experimental mice receiving ganciclovir at E11–E13, but not thereafter, had the defective phenotype. Ganciclovir had no effect on control mice regardless of age at treatment.

The magnitude of the components of the defective neocortical phenotype in ablated mice were ganciclovir dose-dependent (i.e. 'smaller' treatments produced less cell death and less severe defects) during the E11–E13 period of vulnerability. Consequently, the qualitative analyses included all of the ablation groups produced during this period to eliminate non-specific and/or non-essential defects from the ablation phenotype. The quantitative analyses, and all examples shown in the Figures, originated from the main ablation group (four ganciclovir treatments on E11 and E12) and the ancillary ablation group that received two ganciclovir treatments on E11 to characterize the maximum extent of specific defects produced in the ablation phenotype. In the latter group, mice were usually terminated on E12 to define the earliest cellular aspects of the ablations.

Targeted ablation produces excess apoptosis in the dorsal pallium

Qualitative regionalization of apoptotic cells

Control and ablated mice had dying cells located in the dorsal pallium from E12 to P4. The mode of cell death in both groups was apoptosis, as signified by pyknosis (chromophilia/shrinkage) and/or TUNEL labelling (Van Cruchten and Van den Broeck, 2002; D'Herde et al., 2003). These indicators were co-localized and yielded similar results, so their data were pooled.

Control and unablated experimental mice had normal backgrounds of diffuse, infrequent apoptotic cells in the dorsal pallium and adjacent neostriatum. Dying cells during early neocorticogenesis were found mostly in the ventricular zone, which dominated the vertical extent of the dorsal pallium from E12 to E14 (Figure 1). Apoptotic cells were

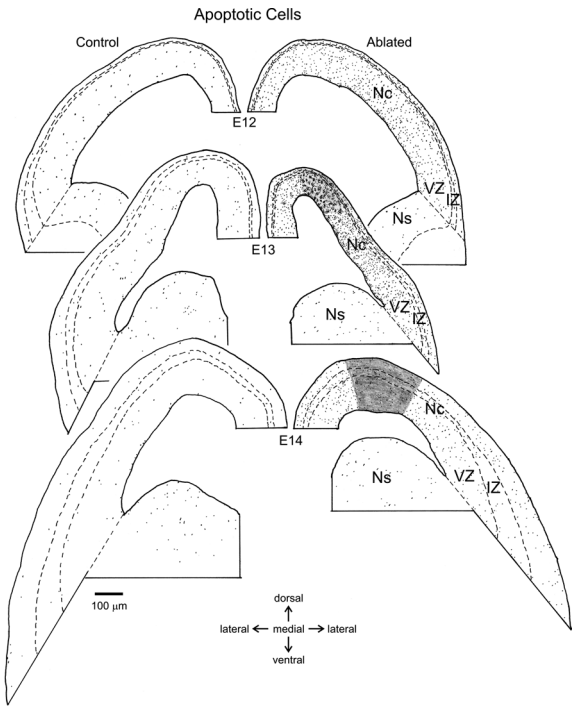

Figure 1 Camera lucida maps of apoptotic cells in coronal sections from control (left-hand side) and ablated mice (right-hand side; E11 and E11–12 ganciclovir treatments) at E12 (top), E13 (middle) and E14 (bottom)
Developmental effects are shown by differences in vertical sequences, with superimposed ablation effects shown by differences in horizontal pairs from same-age littermates. Pairs are arranged as mirror-images to reveal asymmetry. Dots are dying cells detected by low-resolution light microscopy (4 × objective, total magnification × 50). Broken lines are borders of intermediate zone and neostriatum. Shaded areas are scars. Nc, neocortex; Ns, neostriatum; VZ, ventricular zone; IZ, intermediate zone. Scale bar=100 μm.

found mostly in the mantle zone after E15. Both brain regions exhibited normal growth with increasing age.

Ablated mice had excess dying cells in restricted parts of forebrain. They rapidly, but transiently, accumulated high levels of apoptotic cells in the dorsal pallium, but not the neostriatum (nor, with certain exceptions, any other forebrain site) during and immediately after ganciclovir treatment from E12 to E14 (Figure 1). These excess apoptotic cells were found mostly in the ventricular zone and, in some cases, were located in distinct regions of unscarred and scarred tissue. Their early accumulation was the initial indicator of the ablation neocortical phenotype, which never occurred in their absence. Growth stalled in the dorsal pallium during their accumulation but resumed with their disappearance. Lower levels of excess apoptosis recurred after E16, long after the termination of effective ganciclovir treatments. These late excess apoptotic cells were found mostly in the mantle zone.

Non-specific apoptosis in ablated mice

The targeted ablation was capable of killing both GPT and non-GPT cells under certain conditions. Four distinct types of non-specific apoptosis of non-GPT cells were recognized. All cells with these types of non-specific apoptosis were excluded from the quantitative analysis. Three of these types were eliminated as necessary contributors to the ablation phenotype, and all regions with these types of non-specific apoptosis were also excluded from the quantitative analysis.

Control mice had very few apoptotic cells combined with macrophages (or comparable histiocytes; resident microglia were not apparent in the dorsal pallium during this early period of development). All groups of ablated mice that received ganciclovir treatment before E13 had approx. 10% of their early-onset apoptotic cells located in unscarred dorsal pallium surrounded by dying macrophages, which often contained small apoptotic bodies, on E13. Assemblies of apoptotic cells and macrophages disappeared by E15, and did not recur during late-onset apoptosis. Early-onset phagocytosis was not sufficient to account for the ablation phenotype, but could not be eliminated by the tested experimental conditions. Its main action was the acceleration of the disappearance of excess apoptotic GPT neurons on E14 (Figure 2A).

Control mice had no scars. Ablated mice in the main group typically (157/160 tested cases) had bilateral scars at the

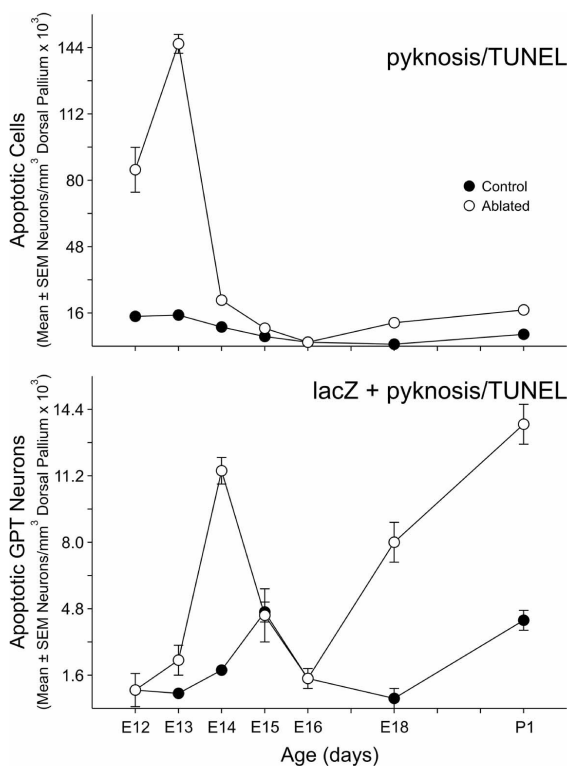

Figure 2 Corrected mean densities ± S.E.M. showing different age-related trends of accumulated apoptotic cells in control and ablated mice from E12 to P1 (E11 and E11–12 ganciclovir treatments)
Top panel: standard measurements of dying cells shown by pyknosis and TUNEL indicators in all vertical zones of dorsal pallium. Bottom panel: standard measurements of dying GPT neurons shown by co-localization of lacZ with pyknosis and TUNEL indicators in marginal and mantle zones.

dorsomedial peak of the dorsal pallium on and after E13 (Figures 1 and 4F). Scars were associated with multiple ganciclovir treatments at <16 h intervals, and were found in >50% of cases with two or more treatments at E11–E13 in ancillary groups with smaller ablations. Scars eventually occupied 10% of the dorsal pallial volume. Nearly all GPT and non-GPT progenitors and neurons were killed in the scars during and shortly after ganciclovir treatment, unlike the adjacent, unscarred dorsal pallium. Apoptosis was multiplicative, and dying cells formed clustered aggregates within the scars. The time-course of apoptotic initiation extended beyond one mitotic cell cycle and was usually accompanied by extensive phagocytosis on E13. Few, if any, progenitors, GPT neurons, cortical plate neurons, astrocytes, oligodendroglia or ependymal cells were generated during subsequent development. Scars were penetrated by fibroblasts, ventricular zones were obliterated and the dorsal pallium thinned after E13. Scars were largely and persistently avascular, with few resident neurons, indistinct marginal/mantle zone boundaries and neuroepithelial collapse.

Scars were not necessary contributors to the ablation phenotype. They did not always accompany ablation even with the most destructive ganciclovir treatments. They were eliminated by increasing the intertreatment intervals of ganciclovir administration. Comparable data were obtained from unscarred cases and unscarred dorsal pallium of scarred cases. However, scars were a significant instructive artefact. They were direct morphological evidence for a distinct outcome in the ablation phenotype due to concurrent, early apoptosis of GPT and non-GPT cells. The alternative, more fundamental, outcome of the unscarred dorsal pallium was due to the specific early apoptosis of GPT cells only, as seen within adjacent regions of dorsal pallium in the same ablated mice and in unscarred ablated mice. This difference demonstrated that non-GPT progenitors and neurons were largely, if not entirely, spared in the unscarred dorsal pallium of ablated mice, although the identities of all non-GPT cells or all apoptotic cells could not be established with absolute certainty due to technical limitations.

Two other defects occurred only in severely scarred ablated mice, and were therefore not necessary contributors to the ablation phenotype. Transient increases of apoptotic neurons were seen in forebrain circumventricular organs, particularly the median eminence, for several days following ganciclovir treatment. Also, ventricular expansion and neocortical thinning occurred after E18 as signs of progressive hydrocephalus (Figure 4F).

Quantitative development of apoptotic cell density

Densities of apoptotic cells in the dorsal pallium of control mice were relatively high at E12–E13 during the generation of GPT cells, but decreased reliably from E12 to E16 before rising slowly to a lower level after E18 (Figure 2A; $P_\alpha<0.05$). Densities of apoptotic cells in the unscarred dorsal pallium (the exclusive focus of further analysis) of ablated mice were reliably greater than in same-age controls (Figure 2A; $P_\alpha<0.05$). These differences represented excess cell death, which emerged in three phases.

The early-onset phase of apoptosis consisted of significant increases in the densities of dying cells from E12 to E15 ($P_\alpha<0.05$). Excess apoptosis was greatest from E11 to E12 during the normal period of generation for GPT cells (+494% of the control value). Continued ganciclovir treatments produced a peak accumulation at E13 (+873% of the control value). Apoptosis decreased rapidly after E13 and was nearly absent at E16. These data indicated that excess apoptotic cells were generated within 12 h, and persisted for approx. 48 h, after ganciclovir treatment, consistent with previous estimates of the time-course of apoptotic cells in normal neocortex (Takahashi et al., 1996). Early-onset apoptosis was due mainly to the death of GPT cells triggered by ganciclovir treatment. Its rapid, additive onset, and even more rapid subsidence, demonstrated that each ganciclovir treatment exerted a killing effect on a cell cohort generated within one cell cycle.

The middle-onset phase of apoptosis matched the low, normal density of dying cells encountered in control mice on E16. Excess apoptosis was absent at this time.

The late-onset phase of apoptosis consisted of reliable increases in the densities of apoptotic cells after E18 ($P_\alpha<0.05$). This recurrent apoptosis was minor in magnitude, with the peak value on P1 at <15% of the peak value for the early-onset phase. Late-onset apoptosis was due to the death of settled neocortical neurons more than 5 days after ganciclovir treatment.

Direct demonstration of apoptotic GPT neurons

Only a small fraction of apoptotic cells was identified by double-labelling as GPT neurons, owing to the destructive processes of cell death, which usually impaired migration and reporter expression.

Apoptotic GPT neurons (lacZ) were seen in the mantle and marginal zones of the dorsal pallium from E12 to P1 in control mice. They were 5% of the total apoptotic cells during the generation of GPT cells seen on E11–E13 and >75% after E15 (Figure 2B).

GPT neurons died during both the early- and late-onset phases of apoptosis in ablated mice. Excess densities of apoptotic GPT neurons were found in the mantle and marginal zones on E13 and E14 ($P_\alpha<0.05$) during and shortly after peak total apoptotic density. They were 2% of the total apoptotic cells (i.e. approximately half of the normal proportion) during the generation of GPT cells seen on E11–E13 in controls and >75% after E15 (Figure 2B). Their initial accumulation was delayed by the time required for apoptotic triggering, migration and settlement. Their presence indicated that ganciclovir-triggered apoptosis did not block mitosis in GPT progenitors committed to apoptosis, nor completely eliminate migration and reporter expression by

GPT neurons. In both control and ablated mice, marginal zones were mostly cleared of GPT neurons after E16, densities of apoptotic GPT neurons in mantle zones increased after E18, and concurrent depletion of GPT and non-GPT neurons occurred during the late-onset phase of excess apoptosis in ablated mice ($P_\alpha < 0.05$).

Many of the early-onset apoptotic cells found in the mantle and marginal zones degenerated so rapidly that their GPT identity could not be directly determined at 24 h after ganciclovir treatment. However, nearly all of these apoptotic cells, including directly identified apoptotic GPT neurons, had a dispersed, non-clustering, isolated pattern of settlement in the preplate and primitive neocortex. They were often located in close proximity to viable GPT neurons, as well as viable candidate (i.e. unlabelled) non-GPT neurons that escaped specific cell killing initiated by ganciclovir treatment during their mitotic generation from progenitors and non-specific killing due to their proximity to dying cells. These morphological findings, and the observed limitation of cell killing to single cell-cycle cohorts of newly proliferated cells, indicated that toxin leakage into GPT or non-GPT neurons mediated little or no non-specific bystander effect on neurons located in the unscarred dorsal pallium.

Targeted ablation delays the organization of viable GPT neurons in the dorsal pallium

Localization of reporters in GPT neurons

Comparable GPT neurons were observed in control and ablated mice. HSV-TK was found in infrequent GPT neurons located in the marginal, mantle and intermediate zones of dorsal pallium in experimental mice, whereas τ-eGFP and lacZ were almost undetectable before ganciclovir treatment on E11. Reporters resided in the perikaryal cytoplasm of far more frequent post-mitotic (G_0-phase) GPT neurons located distal to the ventricular zone in dorsal pallium from E12 to P4 (Figures 3, 4 and 12). GPT neurons had fusiform or multipolar cell bodies, somatic diameters >7 μm and dispersed nuclear chromatin. Somatic diameters grew to >10 μm, and τ-eGFP labelling extended into dendritic and axonal processes in older mice.

Apoptotic GPT neurons which localized with each of the reporters were settled in the marginal and mantle zones of control and ablated mice at E12–P4. These cells were most numerous on E12–E14 in ablated mice, and reflected the early-onset phase of ganciclovir-induced apoptosis. The cellular profiles of apoptotic GPT neurons were similar in control and ablated mice and, with allowance for pyknotic

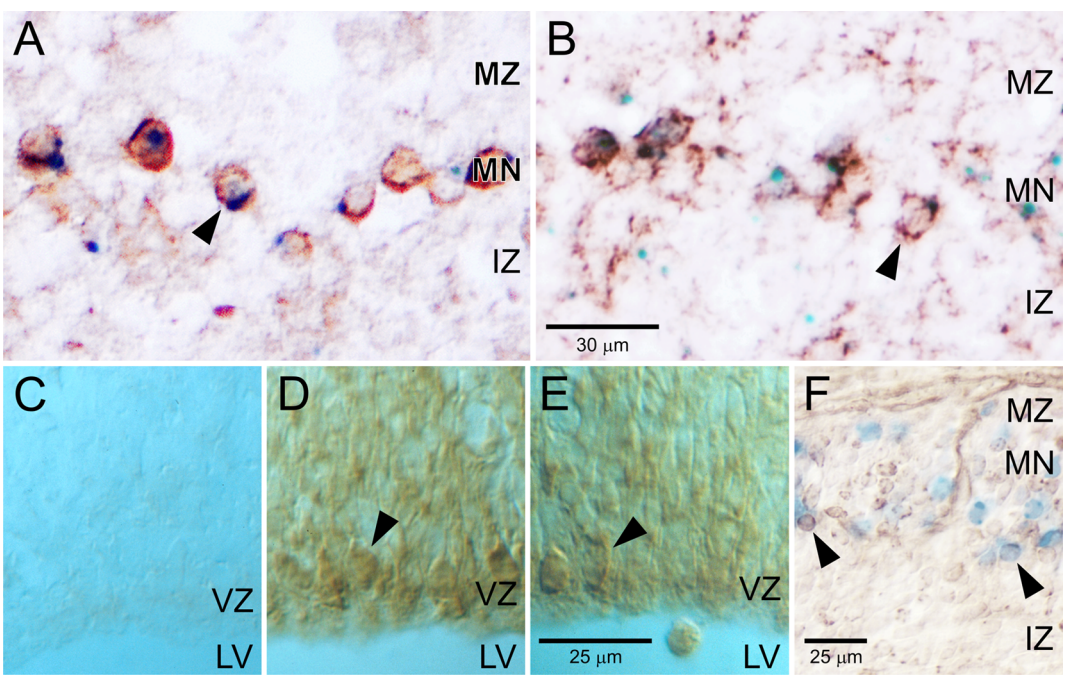

Figure 3 Photomicrographs of GPT neurons and neuroblasts

(**A**) Co-localization of lacZ (blue) and HSV-TK (brown) in a GPT neuron (arrowhead) of an E13 unablated experimental mouse. (**B**) Co-localization of lacZ (blue) and τ-eGFP (brown) in a GPT neuron (arrowhead) of an adjacent serial section from same mouse. Scale bar=30 μm for (**A**) and (**B**). (**C**) Lack of HSV-TK-immunoreactive cells in the dorsal pallial ventricular zone of an E12 control mouse. (**D**) HSV-TK immunoreactive cells (GPT neuroblasts; arrowhead) in dorsal pallial ventricular zone of an E12 unablated experimental mouse. (**E**) HSV-TK immunoreactive cells (GPT neuroblasts; arrowhead) in dorsal pallial ventricular zone from an E12 ablated experimental mouse (E11 ganciclovir treatment). Scale bar=25 μm for (**C**)–(**E**). (**F**) Co-localization of lacZ (blue) and BrdU (brown) in GPT neurons (arrowheads) generated on E13 in an E15 control mouse. Scale bar=25 μm for (**F**). MZ, marginal zone; MN, mantle zone; IZ, intermediate zone; VZ, ventricular zone; LV, lateral ventricle.

shrinkage, resembled viable GPT neurons within each age group.

GPT neurons were the predominant cells in preplate neocortex in control mice at E12–E13. Adjacent sections singly labelled for each reporter showed that approx. 30% of the cells in the marginal zone in unablated triple-transgenic experimental mice were GPT neurons, with similar results for τ-eGFP and lacZ in control mice during this early period. More than 90% of the cells in the mantle zone of the same sections were GPT neurons. Reporter co-localizations were observed directly in nearly 90% of GPT neurons at E12–E13 (Figures 3A and 3B) in adjacent sections labelled for HSV-TK+lacZ and τ-eGFP+lacZ in triple-transgenic unablated experimental mice. The proportions of GPT neurons were reduced to $<$10% of the neurons in the marginal zone and $<$50% of the neurons in the mantle zone during this period in ablated experimental mice. They retained normal levels of non-GPT neurons, which transiently increased their density due to the paucity of viable GPT neurons. This result indicated that non-GPT neurons were not subjected to significant non-specific killing in the unscarred neocortex of ablated mice.

Viable and dying GPT neurons of control and ablated mice settled in the dorsal pallium by and after E11 in agreement with molecular biological evidence (Landry et al., 1998). All three reporters were detected in neocortical neurons that matched, with no evidence for reporter leakage, the structure of GPT neurons shown by *in situ* hybridization (Jacobs et al., 2007). Localization of any of these reporters in GPT neurons was a surrogate for the others, as predicted by genotype. Hemi- and homozygous offspring, like homozygous progenitors, had similar results for τ-eGFP and lacZ transgenes, so their data were pooled. Double- and triple-transgenic mice had identical results for shared transgenes, so their data were pooled when appropriate.

Regional organization of GPT neurons

The vertical organization of GPT neurons in control mice emerged with their settlement in the mantle and marginal zones of preplate neocortex (Figures 4A, 4C and 4E). The primordial, unilaminar settlement of GPT neurons in the preplate neocortex established superficial (marginal zone), middle (mantle zone intercalated with cortical plate) and deep (mantle zone subplate) laminae in primitive neocortex from E13 to E15. This trilaminar pattern persisted in mature neocortex at E16, with separation of the distal laminae by intervening supragranular cortical plate neurons and separation of the proximal laminae by expansion of the fibrous band of layer VI. Normal apoptosis of GPT neurons from E16 to P4 followed a distal (early)-to-proximal (late) sequence, and eventually restricted these cells mostly to the subplate and deep parts of layer VI.

The horizontal organization of GPT neurons in control mice began to emerge on E12 with their first settlement near the rhinal sulcus (Figure 4A). This region became juxtallocortex, with the greatest density of GPT neurons in forebrain. Subsequent, concentric, settlement of GPT neurons into neo- and allo-cortex was finished by E16. Approx. 50% settled into neocortex in a lateral (early)-to-medial (late) neurogenetic gradient. The remainder settled into juxtallo- and allo-cortex, with small contributions to claustrum and amygdala. No other forebrain sites contained GPT neurons.

Ablated mice had the same patterns of vertical and horizontal organization of GPT neurons as control mice (Figures 4B, 4D and 4F). They required one or two additional days of age to complete the settlement of GPT neurons into preplate neocortex before its structural transformation into primitive neocortex. The middle and deep laminar distributions of GPT neurons were more diffuse and disaggregated in ablated mice during the postnatal period. This defect was accentuated in scarred, hydrocephalic cases, which suggested the occurrence of a non-specific disruption in the orderly apoptotic sequence found in control mice (Figures 4E and 4F).

Qualitative distribution of GPT neurons

The density of GPT neurons (lacZ) in control mice increased from their initial detection at E12 and peaked at E16 as their generation and accumulation outpaced volumetric tissue growth (Figures 4A, 4C and 4E). GPT neurons became sparser after E16 due to cessation of generation and accumulation, continued neocortical growth and normally accelerated apoptosis.

GPT neurons (lacZ) in ablated mice were also first detected at E12, but their density did not increase notably until E14 (Figures 4B, 4D and 4F) with the subsidence of early-onset apoptosis in unscarred dorsal pallium. They became denser than in controls, as extended generation led to excess accumulation relative to volumetric tissue growth between E14 and E16. They became sparser than in controls after E16 due to cessation of generation and accumulation, continued neocortical growth and abnormally accelerated, late-onset apoptosis.

Targeted ablation delayed the accumulation of viable GPT neurons in unscarred neocortex in patterns that mirrored the regional accumulation of early-onset apoptotic cells in the mantle zone and its underlying intermediate and ventricular zones (i.e. along the radial path of migration and settlement of GPT neurons). The simultaneous shortfall of distal, viable GPT neurons and the excess accumulation of proximal, dying cells was indirect anatomical evidence that a substantial fraction of the apoptotic cells was morphologically related to GPT neurons.

Quantitative density of GPT neurons

The density of viable GPT neurons in the dorsal pallium of control mice was a parabolic function of age (Figure 5). It represented the generation and settlement of GPT neurons as an early rising phase followed by continued tissue growth and neuronal loss during a late descending phase. GPT neurons (lacZ) in control mice showed reliable daily increases in

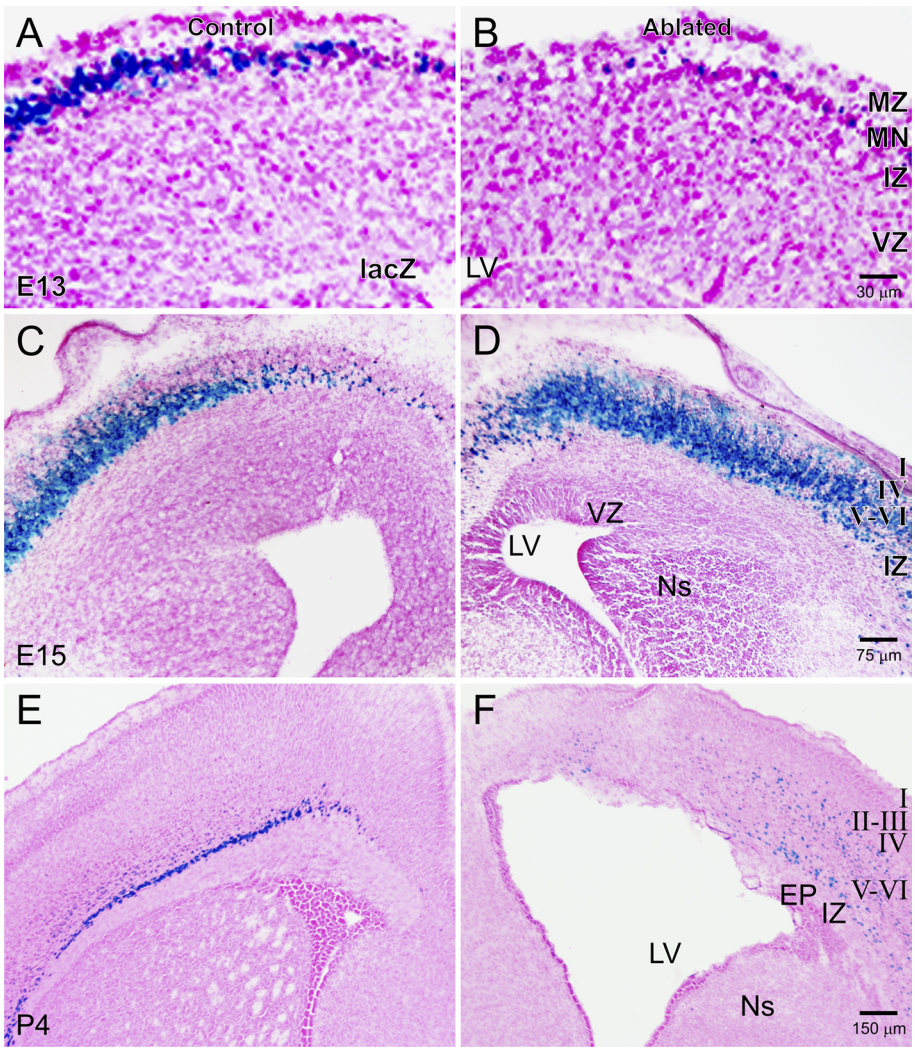

Figure 4 Photomicrographs of the organization of GPT neurons (blue, lacZ) in coronal sections of dorsal pallium counterstained with Neutral Red in control (A, C and E) and littermate ablated (B, D and F; E11 and E11–E12 ganciclovir treatments) mice

Developmental effects are shown by differences in vertical sequences, and superimposed ablation effects are shown by differences in horizontal pairs. Pairs are arranged as mirror-images to reveal asymmetry. (**A** and **B**) Early phase suppressed accumulation of GPT neurons in E13 ablated neocortex. MZ, marginal zone; MN, mantle zone (preplate); IZ, intermediate zone; VZ, ventricular zone; LV, lateral ventricle. Scale bar=30 μm. (**C** and **D**) Middle phase exuberant replacement of GPT neurons in E15 ablated neocortex. I, molecular layer; IV, granular layer; V–VI, infragranular layers; IZ, intermediate zone; VZ, ventricular zone; LV, lateral ventricle; Ns, neostriatum. Scale bar=75 μm. (**E** and **F**) Late phase dissolution of GPT neurons in P4 ablated neocortex. Hydrocephalus, pallial thinning, dyslamination and diffuse arrangement of surviving GPT neurons are apparent in this older ablated mouse. The progressive reduction of cell density associated with hydrocephalus make the scattered distal GPT neurons more apparent than in the control mouse, even though their normal laminar distribution is maintained. Note the central scarred region, its grossly reduced cellularity and the absence of the deep layer VI subplate of GPT neurons within it. I, molecular layer; II–III, supragranular layers; IV, granular layer; V–VI, infragranular layers; IZ, intermediate zone; EP, ependymal layer; LV, lateral ventricle; Ns, neostriatum. Scale bar=150 μm.

density from E12 to E16, and a reliable cumulative increase of +650% during the early phase ($P_\alpha<0.05$). A cumulative decrease of −62% from E16 to P4 was statistically significant ($P_\alpha<0.05$), and showed the normal recision of GPT neurons during late development.

Comprehensive and standard measurements of GPT neurons (lacZ) yielded similar density values at each age level ($P_\alpha>0.05$). However, standard density values obtained for GPT neurons (HSV-TK and τ-eGFP) in unablated experimental mice showed the initial rising phase between E11 and E14, and a peak value at E14 equivalent to the lacZ peak value at E16. Similar late-phase decreases after E16 were obtained with all three reporters (Figure 5). Thus lacZ was less efficient than HSV-TK and τ-eGFP reporters during the early, but not the late, development of GPT neurons. These data indicated that neocortical GPT neurons were normally acquired from E11 to E14, consistent with the vulnerability of GPT cells to ganciclovir-induced apoptosis from E11 to E13, plus a delay of 24 h for migration and settlement.

The density of viable GPT neurons in the unscarred dorsal pallium of ablated mice retained the same developmental pattern, but had a reliably different age distribution from

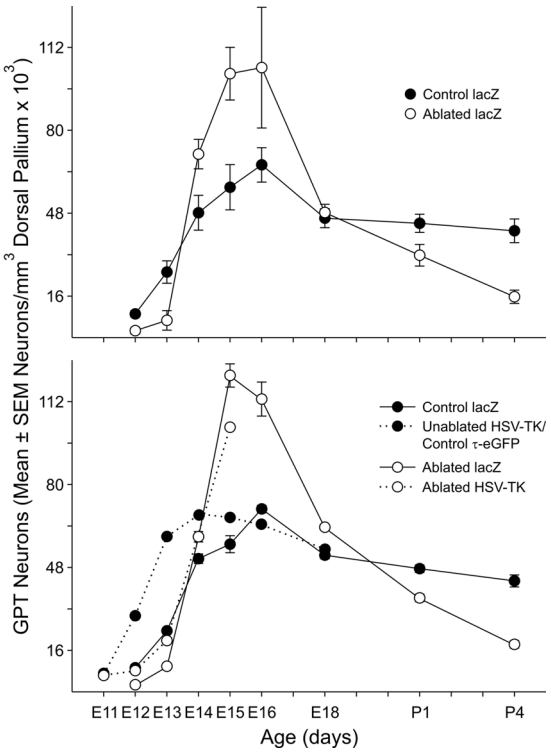

Figure 5 Corrected means ± S.E.M. of GPT neurons in the marginal and mantle zones of dorsal pallium in control and ablated mice from E11 to P4 (E11 and E11–E12 ganciclovir treatments)

Top panel: comprehensive measurements of age-related differences of accumulated GPT neurons [lacZ (Neutral Red counterstain)] in control and ablated groups. Bottom panel: standard measurements of age-related differences of accumulated GPT neurons [lacZ (haematoxylin counterstain), HSV-TK and/or τ-eGFP in control and ablated groups.

that of controls (Figure 5; $P_\alpha<0.05$). The early rising phase was extended, which skewed the distribution to the right. The distribution was also more kurtotic, with greater peak density and accelerated rising and descending phases. Comprehensive and standard measurements of GPT neurons (lacZ) again yielded similar values ($P_\alpha>0.05$). Standard density values obtained for GPT neurons (HSV-TK) showed a cumulative increase for the rising phase, a peak value at E15 that approached the lacZ peak value and a late descending phase as for control mice (Figure 5). GPT neurons were acquired approx. 2 days later in ablated mice than in control mice for all reporters.

This pathogenetic sequence had a first phase of suppression of GPT neurons (E12–E13; Figures 4A and 4B). Ablated mice had a reliably lower density of viable GPT neurons than controls during the early-onset phase of ganciclovir-induce apoptosis (compare Figures 2A and 5A; $P_\alpha<0.05$).

The second phase was signified by an unpredicted, exuberant replacement of GPT neurons (E14–E16; Figures 4C and 4D). Ablated mice had a reliably higher density of viable GPT neurons than controls, which peaked at E15–E16 during the middle phase of normal background apoptosis (compare Figures 2A and 5A; $P_\alpha<0.05$). Reliable daily increases in density were observed from E12 to E16 ($P_\alpha<0.05$). Peak densities were reliably greater in ablated mice than controls at E15–E16 (+65%; $P_\alpha<0.05$).

Local increases in the density of GPT neurons/tissue unit during the second phase were not reflected in the total frequency of GPT neurons/hemisphere due to persistent growth impairment in ablated mice. The maximum complements of GPT neurons/hemisphere were 1.28×10^5 for control mice and 1.12×10^5 for ablated mice ($P_\alpha>0.05$) upon expansion by the volume of dorsal pallium devoted to neocortex as reconstructed from serial sections at peak ages for GPT neuron density. The 12% shortfall of GPT neurons in ablated mice approximated the 10% loss of dorsal pallium and its proliferative ventricular zone due to scars. The recovery of a relatively normal total complement of GPT neurons in ablated mice, gained by the proliferation of surviving GPT neuroblasts and replacement GPT neuroblasts (see below), indicated that dying GPT neurons were unable to rejoin the pool of viable GPT neurons. There were no apparent shortfalls beyond scar losses among non-GPT cells generated subsequent to targeted ablations, except in association with the late occurrence of hydrocephalus.

The third phase showed the dissolution of GPT neurons (E18–P4; Figures 4E and 4F). Ablated mice reverted to lower densities of viable GPT neurons, with reliable differences from controls at P1–P4 (compare Figures 2A and 5A; $P_\alpha<0.05$) corresponding with the late-onset phase of excess apoptosis. The cumulative decreases for this late period reliably exceeded comparable control values (−85%; $P_\alpha<0.05$).

Targeted ablation altered the density, as well as the distribution, of viable GPT neurons within developing neocortex in patterns that mirrored the density of apoptotic cells in the mantle, intermediate and ventricular zones. The quantitative coincidence and covariation between the predominant fate of live GPT neurons and the early-onset dying cells was further indirect evidence for the identity of apoptotic GPT cells in ablated mice. Many live GPT neurons were missing during early-onset apoptosis in ablated mice due to their failed generation from dying progenitors or their transformation into dying GPT neurons.

Targeted ablation reconstitutes the ventricular zone to replace GPT neuroblasts and GPT neurons in the dorsal pallium

Localization of reporters in GPT cells in the ventricular zone

All three reporters demonstrated that GPT neurons settled in the marginal and mantle zones, but only HSV-TK allowed them to be traced back to their immediate progenitors. These cells were found exclusively in the ventricular zone of the dorsal pallium in E11–E13 unablated and E11–E15 ablated experimental mice (Figures 3C–3E). They were absent from control mice and all other forebrain ventricular zones in experimental mice.

Ganciclovir-induced apoptosis was produced only during the period when these cells were observed in experimental mice. Approx. 50% of the HSV-TK immunoreactive cells at their peak density in the ventricular zone had condensed nuclear chromatin in counterstained sections. Approx. 15% of these cells had mitotic chromosomal arrays and were interspersed among unlabelled mitotic cells when adjacent to or within 25 μm of the ventricular lumen. Taken together, these cells were GPT progenitors in S-, G_2- and mitotic cell-cycle phases immediately before separation of asymmetrically divided daughter GPT neurons and neuroblasts, or symmetrically divided daughter GPT neurons. Densities of GPT neuroblasts increased and then decreased rapidly during early neocorticogenesis, with peaks at E12 (absent by E14) in unablated experimental mice and E13 (absent by E16) in ablated experimental mice. These nascent periods preceded, then briefly accompanied, the subsequent settlement of GPT neurons in the marginal and mantle zones.

Other GPT cells, usually distal to the lumen in the ventricular zone, had dispersed nuclear chromatin. They were post-mitotic (G_0-phase) GPT neurons in migratory transit from their periventricular mitotic origins and, in at least some cases, pre-mitotic (G_0- or G_1-phase) GPT neuroblasts preparing to re-enter the cell cycle in the distal ventricular zone. They disappeared from the ventricular zone with the mitotic exhaustion and disappearance of GPT neuroblasts. They were supplanted by the normal succession of non-GPT progenitors, which yielded no apparent shortfalls for non-GPT cell types generated subsequent to targeted ablations in the same ventricular zones of the dorsal pallium.

GPT neuroblasts in the S-, G_2- or mitotic phases did not exhibit apoptosis in control or ablated mice. However, their densities were transiently suppressed during the onset of the rising phase of early-onset apoptosis in ablated mice. All of the apoptotic GPT cells in the ventricular zone were G_0- or G_1-phase cells in both control and ablated mice. There were wide variations of TUNEL and HSV-TK label densities in these apoptotic cells in the ablated mice owing to variable durations of ganciclovir exposure during their S-phase period of vulnerability. The tissue densities of these apoptotic cells increased excessively during the early-onset phase of apoptosis in ablated mice when the density of viable GPT cells in the ventricular zone was first suppressed. The initial suppression of mitotically active GPT cells in ablated mice provided direct evidence that a substantial fraction of the dying, non-mitotic GPT cells in the ventricular zone consisted of GPT neuroblasts unable to re-enter the cell cycle. The remainder of the dying GPT cells, half or more of the total dying GPT cells in the ventricular zone of ablated mice, necessarily consisted of GPT neurons (i.e. daughter neurons of asymmetric or symmetric division of GPT neuroblasts) largely unable to migrate into the mantle zone. Both of these outcomes would have contributed to the early shortfall of live GPT neurons settled distally into the marginal and mantle zones.

Many of the early-onset apoptotic cells found in the ventricular zone degenerated so rapidly that their GPT identity could not be directly determined at 24 h after ganciclovir treatment. However, these apoptotic cells, including directly identified apoptotic GPT cells, retained the same dispersed, non-clustering, isolated pattern of distribution found for dying GPT neurons in the mantle and marginal zones. They were located in close proximity to viable GPT cells as well as unlabelled non-GPT cells that escaped specific cell killing. These results, and the observed limitation of cell killing to single cell-cycle cohorts of newly proliferated cells, indicated that toxin leakage mediated little or no non-specific bystander effect on GPT and non-GPT progenitors, as well as GPT neurons, within the ventricular zone of the unscarred dorsal pallium of ablated mice.

Reorganization of the periventricular mitotic array in ablated mice

The periventricular mitotic array near the ventricular lumen appeared to be continuous and only one to three cells deep in 'thick' 20 μm sections at E12–E14 in control mice, although cell density within the array increased with age (Figures 6A and 6B). GPT neuroblasts disappeared as their proliferation of GPT neurons was exhausted.

The majority of periventricular mitotic cells consisted of GPT neuroblasts at E12 in unablated experimental mice. The magnitude of this progenitor population was consistent with the observed high yield of GPT neurons at this time. It was also congruent with the modest growth of the ventricular zone from E11 to E14 (<50% daily volume increase) observed and predicted by a predominant mode of asymmetric division among GPT neuroblasts. Fewer than 10% of the mitotic cells were GPT neuroblasts on E13, and they were absent at E15 (Figure 6A). The density of GPT neuroblasts was reduced at E12 in ablated experimental mice coincident with early-onset apoptosis, the observed low yield of viable GPT neurons and reduced growth of the ventricular zone (<10% daily volume increase) (Figures 6A and 6B). The density of mitotic cells was decreased at the ventricular lumen, but increased overall with the vertical expansion of the full periventricular mitotic array. This transformation was initially signified by the retention of normal levels of non-GPT progenitors and mitotic profiles adjacent to the ventricular lumen and an overall increase in their density within the full extent of the reorganizing mitotic arrays. These results indicated that non-GPT progenitors were not subjected to significant non-specific killing (Figure 6). Subsequently, increased densities of GPT neuroblasts clustered in thickened mitotic arrays, but did not account for their full complement at E13. The peak density of GPT neuroblasts slightly preceded, then accompanied, the exuberant accumulation of GPT neurons. GPT neuroblasts disappeared at E15 before the late-onset dissolution of GPT neurons.

The periventricular mitotic arrays were disrupted by cell-sparse spaces due to apoptosis of entrapped G_0- or G_1-phase GPT cells at E12–E13 in ablated mice. The depth of the damaged arrays increased with age and was reliably greater in

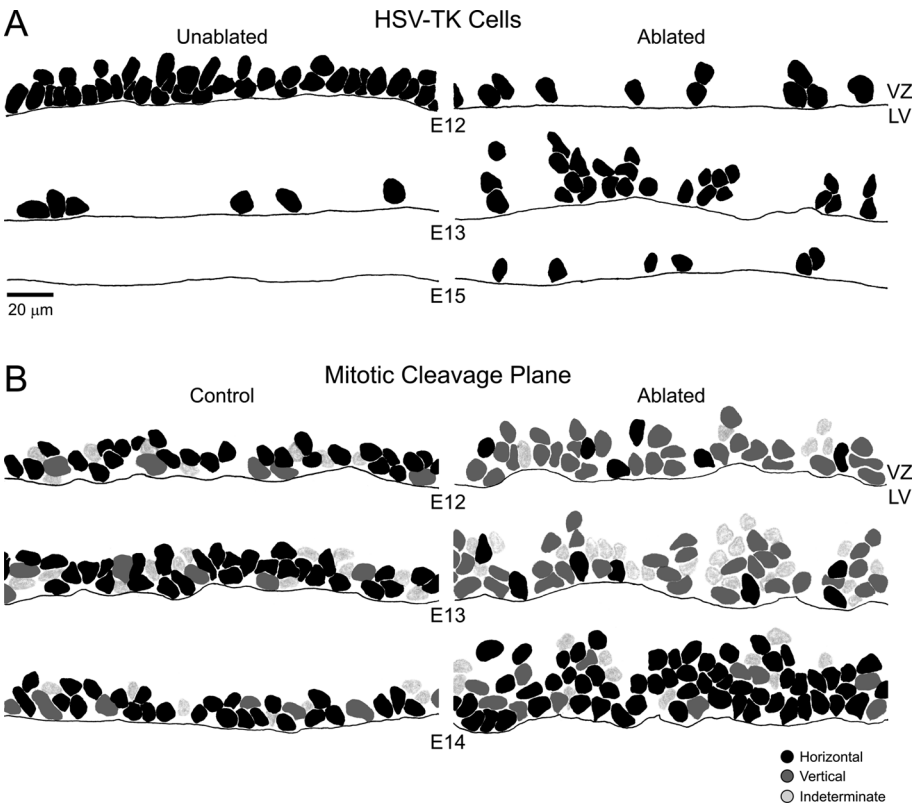

Figure 6 Camera lucida drawings of the organization of proliferative arrays of the dorsal pallial ventricular zone in control, unablated experimental and ablated experimental mice (E11 and E11–E12 ganciclovir treatments)

Developmental effects are shown by differences in vertical sequences, with superimposed ablation effects shown by differences in horizontal pairs from same-age mice. (**A**) Periventricular HSV-TK-immunoreactive cells (GPT neuroblasts) in unablated experimental mice (left-hand panel) and ablated experimental mice (right-hand panel) on E12 (top), E13 (middle) and E15 (bottom). (**B**) Periventricular mitotic cells with horizontal cleavage planes (black), vertical cleavage planes (dark grey) and undetermined (prophase) cleavage planes (light grey) in control (left-hand panel) and ablated experimental mice (right-hand panel) on E12 (top), E13 (middle) and E14 (bottom). VZ, ventricular zone; LV, lateral ventricle. Scale bar=20 μm.

ablated mice than in controls at E12–E14 (Figures 6B; 3–5 $\pm$ 1 compared with 2 $\pm$ 1 cells, $P_{\alpha}<0.05$). Separate, paraventricular mitotic cells were infrequent in both groups during this period.

The reconstitution of the mitotic array was reflected among progenitors positioned adjacent to the ventricular lumen in the dorsal pallium. Control mice had a reliable increase in the density of mitotic cells between E12 and E14 (+28%; $P_{\alpha}<0.05$; Figure 7A), which also enlarged their ventricular surface occupancy (75% at E12 to 96% at E14). Densities of mitotic cells were reliably reduced by −23% on E12 and −53% on E13 ($P_{\alpha}<0.05$) during the suppression stage of GPT neurons in ablated mice, but regained a normal value on E14, coincident with transition to the expansion stage of GPT neurons ($P_{\alpha}>0.05$). The ventricular surface occupancy of mitotic cells dropped to 58% on E12 and 47% on E13, but regained a near-normal value of 93% on E14. Approx. 80% of the mitotic cells were in MAT, with the remainder in prophase in both control and ablated mice at E12–E14 (Figure 7B).

The horizontal cleavage plane was dominant for mitotic MAT neuroblasts in control mice at E12–E14 (81–84% of MAT cells; Figure 6B). More than 95% of the MAT GPT neuroblasts (HSV-TK) counterstained with haematoxylin in unablated experimental mice had the horizontal cleavage plane at these ages. In contrast, more than 95% of the MAT non-GPT progenitors had the vertical cleavage plane. The dominant cleavage plane of MAT cells was reliably altered in ablated mice ($P_{\alpha}<0.05$; Figures 7C and 7D). The vertical cleavage plane was dominant in ablated mice on E12–E13 (84% and 81% of MAT cells respectively; Figure 6B). Fewer than 30% of MAT GPT neuroblasts had the horizontal cleavage plane at these ages. More than 70% of MAT GPT neuroblasts (HSV-TK) and >95% of MAT non-GPT progenitors had the vertical cleavage plane. The horizontal cleavage plane regained its normal dominance at E14 (78% of MAT cells; $P_{\alpha}>0.05$; Figure 6B). Neither cleavage plane was dominant after E14 in control or ablated mice.

The observed values for asymmetric cell division in control mice were larger than those given in previous reports for periventricular, but not paraventricular, anaphase and telophase profiles (Smart, 1973; Haydar et al., 2003). However, the normal dominance of asymmetric division in E12–E14 mice was congruent with the early growth rate of

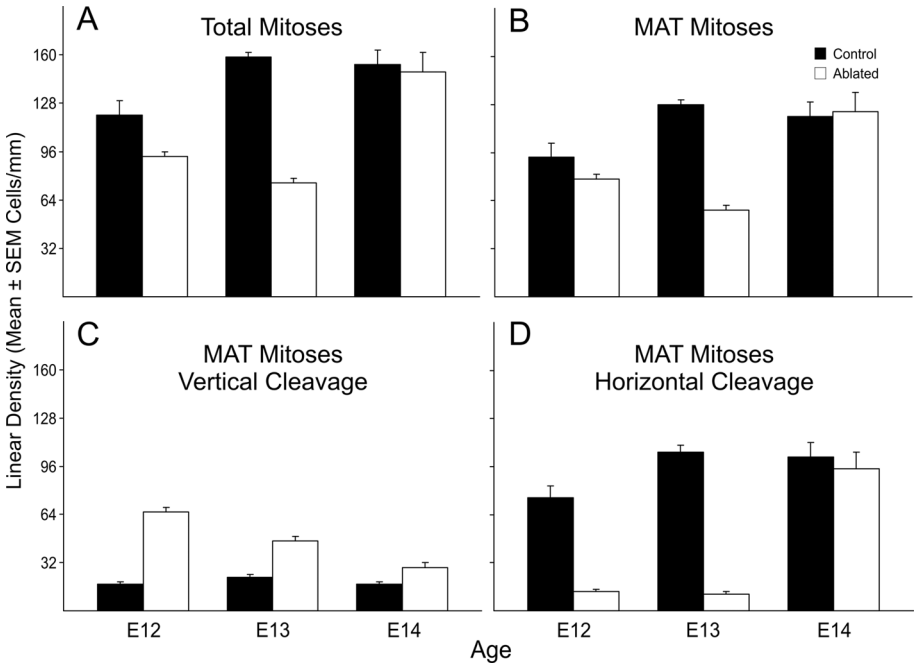

Figure 7 Corrected mean linear densities ± S.E.M. showing different distributions of categories of mitotic profiles at the luminal surface of the ventricular zone proliferative matrix for dorsal pallium in E12–E14 control and ablated mice (E11 and E11–E12 ganciclovir treatments)
(**A**) Total mitotic profiles regardless of phase of mitosis. (**B**) MAT mitotic profiles. (**C**) MAT mitotic profiles with vertical cleavage plane. (**D**) MAT mitotic profiles with horizontal cleavage plane.

the ventricular zone and the accumulation of GPT neurons when the cell-leaving fraction Q was adjusted for the distal expansion of radial migration of GPT neurons beyond the strict boundaries of neocortex (Takahashi et al., 1996). In any event, targeted ablation transiently shifted all mitotic cells toward the vertical cleavage plane, including mitotic GPT neuroblasts.

These observations provided indirect evidence that GPT neuroblasts, as well as GPT neurons, were included among the early-onset apoptotic cells located in the ventricular zone of ablated mice. The density of mitotic GPT neuroblasts was reduced at the ventricular lumen and shifted toward a symmetric division plane during early-onset apoptosis, whereas the density of mitotic non-GPT neuroblasts with a dominant symmetric division plane was reduced at the ventricular lumen, but increased with the thickening of the proliferative array. Thus non-GPT progenitors were spared from non-specific bystander killing and stimulated to proliferate by the targeted ablation of GPT neuroblasts. This outcome was accompanied by a shortfall of distal, viable GPT neurons and an accumulation of nearly twice as many proximal, dying cells, which had to consist of GPT neuroblasts, as well as GPT neurons.

Proliferative replacement of GPT neuroblasts and neurons in the dorsal pallium of ablated mice

The proliferation of non-GPT progenitors allowed the ongoing replacement and additive cell death of GPT neuroblasts and neurons during and shortly after the initiation of early-onset apoptosis in ablated mice. The retention of this proliferative capacity in ablated mice indicated that non-GPT progenitors were not subjected to significant non-specific killing. The subsequent, exclusive origins and radial migration of normal, surviving and replacement GPT neurons from GPT neuroblasts in the ventricular zone of the dorsal pallium were cross-validated by mapping 'birth-dated' BrdU-labelled cells into a developmental neocortical mosaic (Figure 3F).

Doubly labelled GPT neurons in control mice were proliferated only by ventricular zone neuroblasts at E11–E13, with peak production at E11–E12 (shown sequentially in Figures 8–10). GPT neurons migrated radially into the marginal and mantle zones within 24 h of proliferation. Nearly all contained detectable lacZ within 48 h of proliferation, consistent with the differential efficiency of HSV-TK and lacZ reporters. GPT neurons settled in a superficial (early)-to-deep (late) (i.e. 'outside-in') neurogenetic gradient as a characteristic pattern of vertical organization.

This neurogenetic gradient was conserved but delayed in ablated mice (Figures 8–10). At E13, the few viable doubly labelled GPT neurons born on E12 settled deep to GPT neurons born before E12. At E14, doubly labelled cells were embedded between singly labelled GPT neurons born before and after E12. At E15–E16, a larger complement of doubly labelled cells born on E13 settled between singly labelled GPT neurons born before and after E13. At E17, only a few doubly labelled neurons born on E15 settled in the subplate.

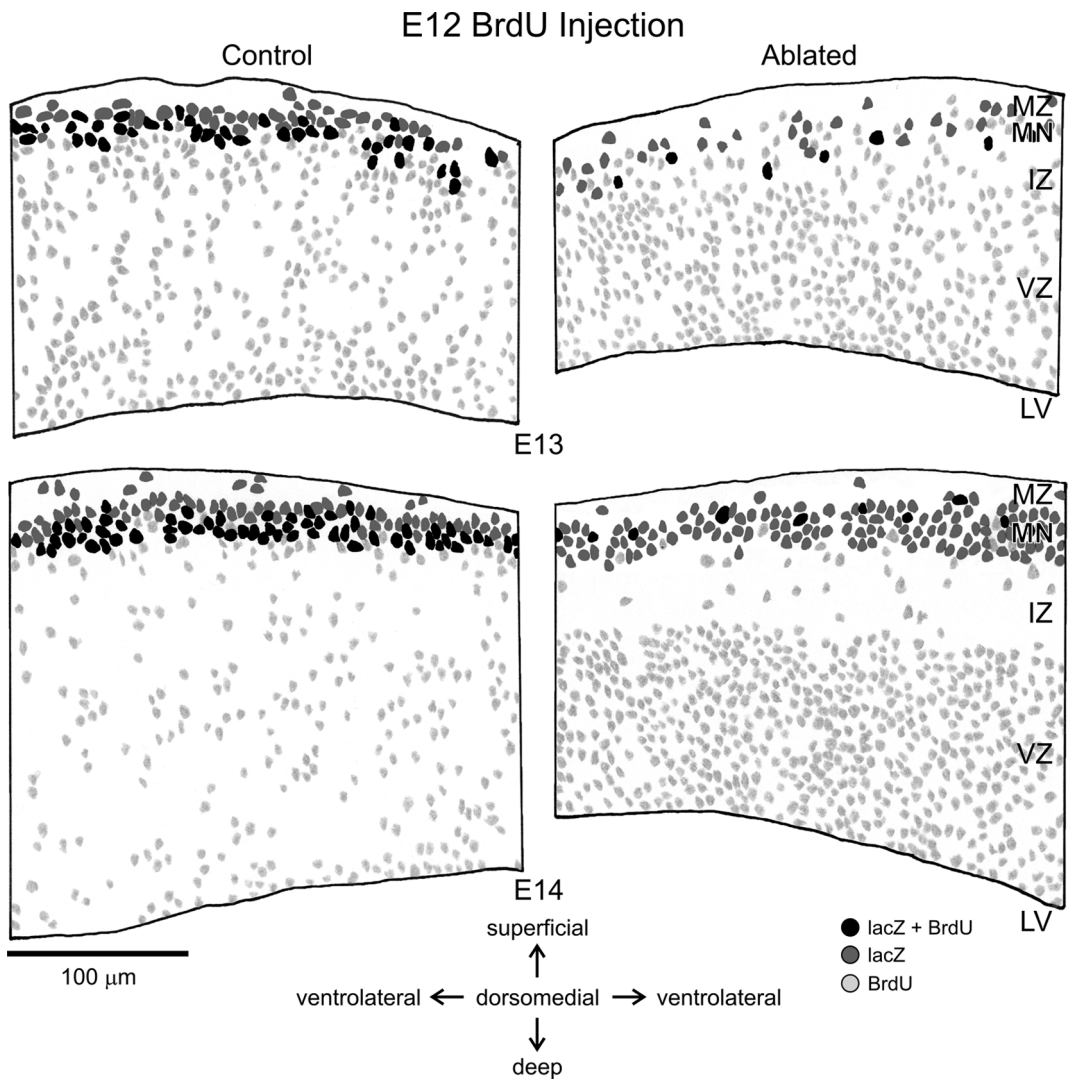

Figure 8 Camera lucida maps of different locations in developing dorsal pallium of doubly labelled GPT neurons (black; BrdU+lacZ) generated on E12, singly labelled GPT neurons (dark grey; lacZ) and singly labelled cells generated on E12 (light grey; BrdU)
Left-hand panels are from control mice and right-hand panels are from littermate ablated mice (E11–E12 ganciclovir treatments). Top panels show positions of labelled cells on E13, 24 h after BrdU administration. Bottom panels show positions of labelled cells on E14, 48 h after BrdU administration. Horizontal pairs are arranged as mirror-images to reveal asymmetry. Compare with Figures 9 and 10 for full developmental sequence. MZ, marginal zone; MN, mantle zone (preplate/cortical plate); IZ, intermediate zone; VZ, ventricular zone; LV, lateral ventricle. Scale bar=100 μm.

A fraction of the BrdU-labelled cells born on E12 in control mice receiving BrdU on E12 migrated into the mantle zone between E13 and E14. Approx. 90% of these cells proved to be GPT neurons, consistent with the dominance of GPT neuroblasts in the underlying ventricular zone during this period (Figure 8). This finding suggested that few, if any, non-GPT neurons originated from either GPT- or non-GPT progenitors in the dorsal pallium before E13. Comparable ablated mice had many persistent, singly labelled BrdU cells in the ventricular zone until E14 (Figure 8). The majority were pyknotic, and accumulated during the early-onset phase of apoptosis. HSV-TK immunolabelling and migration usually failed in these apoptotic cells during the reorganization of the ventricular zone at E12–E13. Ganciclovir-induced apoptosis, which had to be initiated during the S-phase, did not block the early incorporation of BrdU into GPT neuroblasts and GPT neurons. The BrdU-labelled cells that successfully migrated into the mantle and marginal zones in ablated mice were almost always pyknotic and/or GPT neurons.

Substantial remainders of viable BrdU-labelled cells in the ventricular zone in control and ablated mice re-entered the cell cycle as progenitors signified by step-wise reductions (i.e. 'diffusion') of their BrdU label density. Most of the newborn singly labelled cells in control mice receiving BrdU on E13 migrated into the mantle zone and began to show the

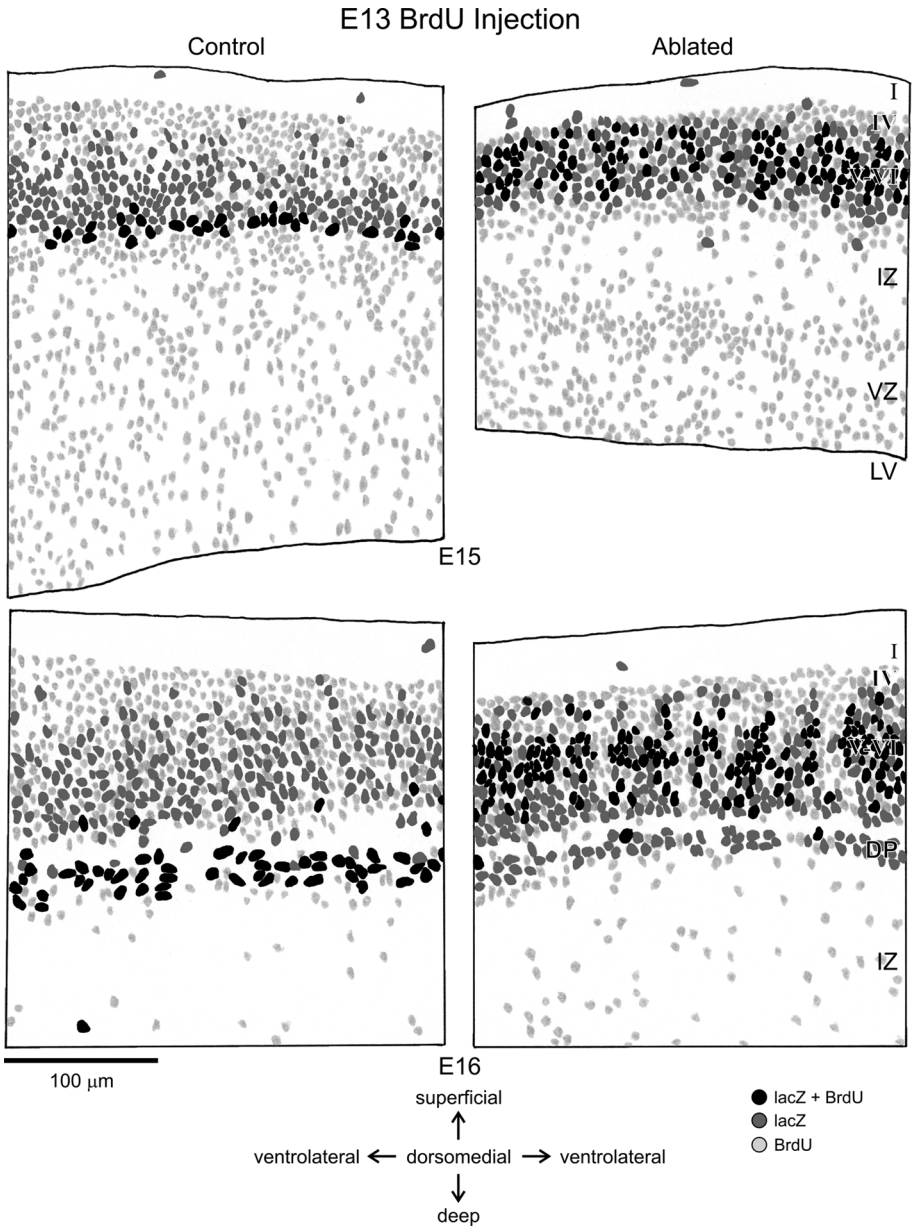

Figure 9 Camera lucida maps of different locations in developing dorsal pallium of doubly labelled GPT neurons (black; BrdU+lacZ) generated on E13, singly labelled GPT neurons (dark grey; lacZ) and singly labelled cells generated on E13 (light grey; BrdU)
Left-hand panels are from control mice and right-hand panels are from littermate ablated mice (E11–E12 ganciclovir treatments). Top panels show positions of labelled cells on E15, 48 h after BrdU administration. Bottom panels show positions of labelled cells on E16, 72 h after BrdU administration. Pairs are arranged as mirror-images to reveal asymmetry. I, molecular layer; IV, granular layer (superficial cortical plate); V–VI, infragranular layers (deep cortical plate); IZ, intermediate zone; VZ, ventricular zone; LV, lateral ventricle. Scale bar=100 μm.

'inside-out' settlement of cortical plate neurons. These cells also began to be born, but to a lesser extent, on E13 in ablated mice. Few singly labelled cells born on E13 after the termination of ganciclovir treatment persisted in the ventricular zone of ablated mice at E15–E16.

Quantitative double-labelling experiments replicated the patterns of normal development and pathogenesis of GPT neurons, but with 10–15% reductions in lacZ label efficiency (compare Figures 5 and 11A). Both densities and percentages of doubly labelled cells showed reliable developmental trends for the normal ages of generation of GPT neurons in control mice and reliable delays in ablated mice (Figure 11; $P_{\alpha}<0.05$). Approx. 50% of the complement of viable GPT neurons in control mice was proliferated by GPT neuroblasts on E12, 10% on E13 and <1% after E13. By extrapolation, 40% was proliferated before E12, mostly on E11. Most of the

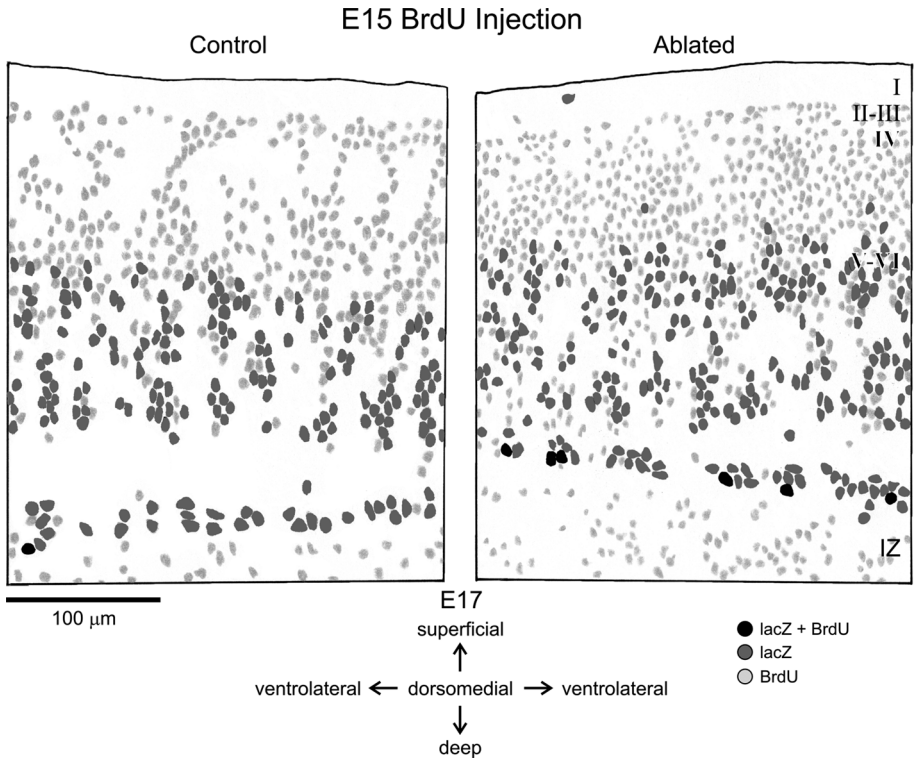

Figure 10 Camera lucida maps of different locations in developing dorsal pallium of doubly labelled GPT neurons (black; BrdU+lacZ) generated on E15, singly labelled GPT neurons (dark grey; lacZ) and singly labelled cells generated on E15 (light grey; BrdU)
Left-hand panel is from a control mouse and right-hand panel is from a littermate ablated mouse (E11–E12 ganciclovir treatments). Panels show positions of labelled cells on E17, 48 h after BrdU administration. I, molecular layer; II–III, supragranular layers; IV, granular layer; V–VI infragranular layers; IZ, intermediate zone. Scale bar=100 μm.

complement of viable GPT neurons in ablated mice was proliferated by GPT neuroblasts after the early-onset phase of ganciclovir-induced apoptosis, as 10% was proliferated on or before E12, 65% on E13 and 10% after E14. By extrapolation, 15% was proliferated on E14. Extension of post-BrdU survival times up to 72 h did not alter the outcome for percentages of doubly labelled neurons for control or ablated mice (Figure 11; $P_{\alpha}>0.05$).

Targeted ablation leads to defective process outgrowth from GPT neurons

All three reporters permitted the detection of GPT neuronal perikarya, but only the τ-eGFP reporter was also localized in their dendritic and axonal cytoplasm from E12 to P4 in control and ablated mice. The outgrowth of dendritic and axonal processes from GPT neurons, best assessed at E18 a few days after settlement and before the advent of gross hydrocephalus in the main group, was reliably impaired in ablated mice ($P_{\alpha}<0.05$). Comparable densities of labelled GPT neurons were present in control and ablated mice at this time, with macroscopic label differences attributed mostly to their processes.

Forebrains of ablated mice had many fewer τ-eGFP labelled processes than littermate controls (Figures 12A and 12B). Moderately impaired dendritic outgrowth of GPT neurons within ablated neocortex accounted for the scarcity of labelled bundles of apical dendrites, commonly seen in controls (Figures 12C and 12D). Mild impoverishment of local collaterals and corticocortical projections from GPT neurons in ablated mice also yielded a diffuse, punctate distribution of labelled axons at the interface of the subplate and corona radiata. Of most significance, labelled corticofugal and corticocortical axonal projections from GPT neurons in ablated mice were infrequent before, on and after E18, and were largely absent from the narrowed fibre fascicles of the internal capsule and thinned corpus callosum (Figures 12E and 12F). Ablated mice had grossly diminished neuropil spaces that would normally have been occupied by thalamocortical axons and neuronal dendrites in layers IV and VI of primary sensory neocortex.

These changes accompanied the late-onset apoptosis of GPT neurons. This phase of cell death did not occur in the presence of ganciclovir, and accompanied, but did not precede or appear to trigger, coincidental cell death among non-GPT neurons in mature neocortex. The apoptotic non-GPT neurons had a wider laminar distribution than GPT

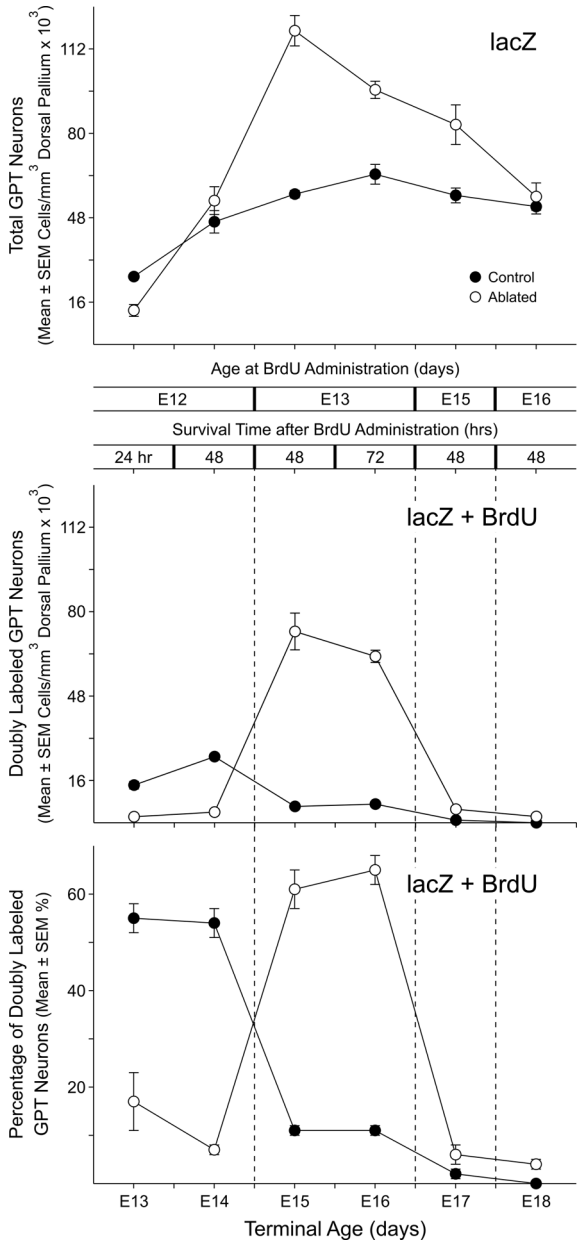

Figure 11 Quantitative analysis of differences of BrdU-labelled GPT neurons in control and ablated mice from E13 to E18 plotted as functions of age at termination and post-BrdU survival (internal axis) (E11–E12 ganciclovir treatments)

Top: corrected mean densities ± S.E.M. (standard measurements) of GPT neurons [lacZ (no counterstain)] in sections doubly labelled for BrdU+lacZ. Middle: corrected mean densities ± S.E.M. (standard measurements) of doubly labelled GPT neurons generated on E12 (left-hand section), E13 (middle section) and E15/E16 (right-hand section). Bottom: mean percentages ± S.E.M. of total GPT neurons doubly labelled on E12 (left-hand section), E13 (middle section) and E15/E16 (right-hand section).

neurons (including supraganular positions), were usually not located in close proximity to apoptotic GPT neurons, and represented a minority of the apoptotic cells within the ablated neocortex.

DISCUSSION

The new observations obtained in the present study show: (i) the normal development of GPT cells, (ii) the targeted ablation of GPT cells predicated on the transient, proliferative phase of their normal development, and (iii) the reactions of surviving and replacement GPT cells predicated on the targeted ablation of their predecessors.

GPT neurons in control mice fulfil all of the morphogenetic criteria now employed for the identification of the principal preplate neurons of mammalian neocortex: radial migration, early proliferation, emission of corticofugal pioneer axons from more deeply settled cells, relatively short survival and an 'outside-in' vertical gradient of settlement (Marin-Padilla, 1971; Bayer and Altman, 1990; Valverde et al., 1995; Verney and Derer, 1995; Meyer and Wahle, 1999; Super and Uylings, 2001; Zecevic and Rakic, 2001). By use of the most sensitive methods available to detect the earliest and widest distribution of these cells, their unilaminar organization in preplate neocortex transforms into a trilaminar organization in primitive and mature neocortex, with a superficial lamina embedded in layer I, a prominent middle lamina engulfed by layers V–VI, and a deep lamina that persists in mature subplate were identified (Landry et al., 1998; Xie et al., 2002: Jacobs et al., 2007; Pontious et al., 2008). The superficial lamina of GPT neurons demonstrates a substantial component of the molecular layer derived by radial migration, while true Cajal–Retzius neurons originate mainly by tangential migration (Bielle et al., 2005). The middle lamina of GPT neurons are definitive preplate neurons, not early-generated infragranular neurons of cortical plate, even in the relatively simple, but highly intercalated, rodent neocortex (Luskin and Shatz, 1985; Hasling et al., 2003). The deep lamina of GPT neurons contains the youngest, but most persistent, of the principal preplate neurons. The developmentally emergent laminar organization of these principal preplate neurons may contribute to the vertical ordering of mature neocortex by positioning selective barriers, or targets, for later-generated neurons, as suggested by reorganization in mutant reeler mice (Sheppard and Pearlman, 1997).

Ganciclovir treatment of age-vulnerable experimental mice bearing the GPT/HSV-TK transgene rapidly initiates a bilateral pathogenetic sequence of increased apoptosis and suppressed accumulation of GPT neurons in neocortex. Targeted to their GPT progenitors, this attack promotes rapid apoptosis of simultaneously proliferated GPT neuroblasts and GPT neurons. Compensatory reconstitution occurs as earlier, invulnerable non-GPT progenitors in the ventricular zone of the dorsal pallium proliferate replacements for killed GPT neuroblasts, which then proliferate replacements for killed GPT neurons. Near-normal restorations of cell complement delay the settlement of GPT neurons into the preplate, which dramatically limits the outgrowth of their axonal projections. Surviving and replacement GPT neurons have the same morphogenetic features as normal GPT neurons, except for

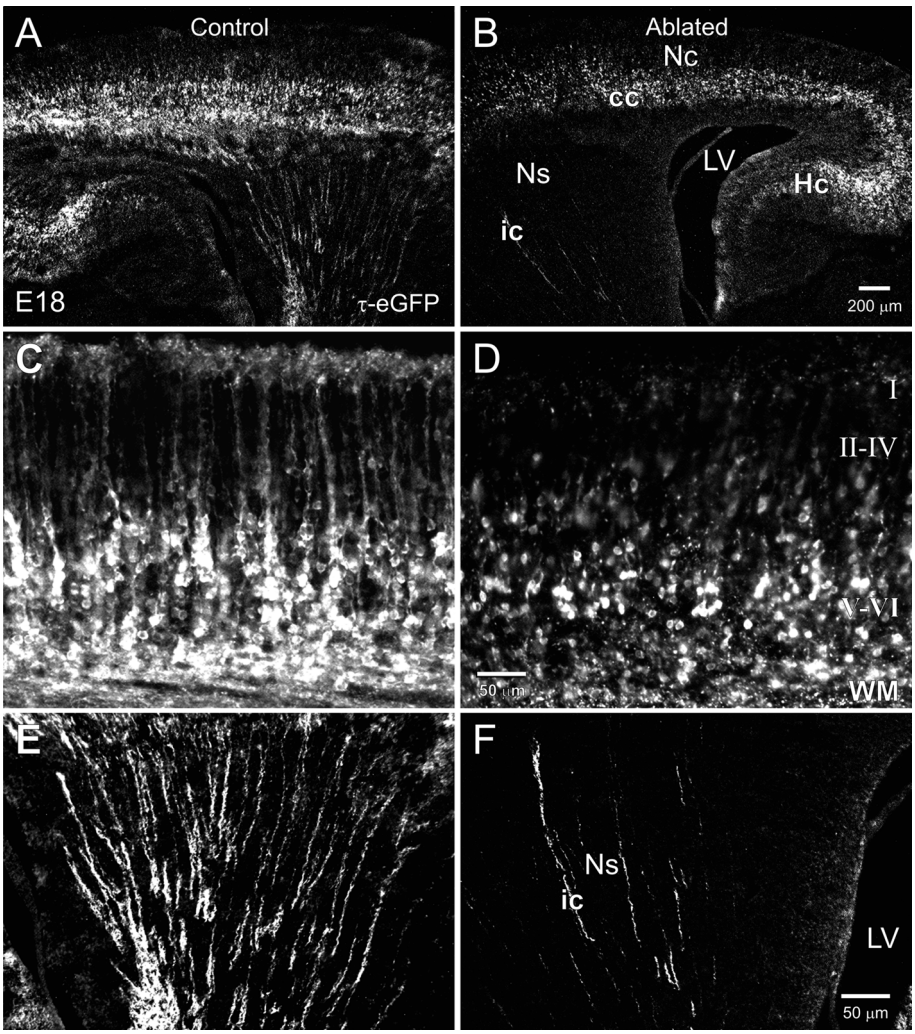

Figure 12 Photomicrographs of sagittal brain sections with fluorescent τ-eGFP label of GPT neurons observed in control (A, C and E) and littermate ablated (B, D and F) mice on E18 (E11–E12 ganciclovir treatments)
Pairs are arranged as mirror-images to reveal asymmetry. (**A** and **B**) Different macroscopic distributions of τ-eGFP-labelled GPT neurons and their processes in control and ablated mice. Nc, neocortex; Ns, neostriatum; Hc, hippocampus; cc, corpus callosum; ic, internal capsule; LV, lateral ventricle. Scale bar=200 μm. (**C** and **D**) Details of different infracortical distributions of τ-eGFP-labelled GPT neurons and their processes in control and ablated mice. I, molecular layer; II–IV, supragranular and granular layers; V–VI, infragranular layers; WM, white matter. Scale bar=50 μm. (**E** and **F**) Details of different distributions of corticofugal pioneer projection axons, emitted by GPT neurons, in fibre fascicles of the internal capsule passing through neostriatum in control and ablated mice. Ns, neostriatum; ic, internal capsule; LV, lateral ventricle. Scale bar=50 μm.

defective axonal outgrowth. The targeted ablation of GPT cells in the dorsal pallium, in concert with the reactions of surviving and replacement cells, yields phenotypic defects of radial migration, laminar framing and afferent guidance, where governance has been attributed to preplate neurons in previous studies (Ghosh and Shatz, 1993; Allendoerfer and Shatz, 1994; McConnell et al., 1994; Molnar and Blakemore, 1995; Ogawa et al., 1995; Del Rio et al., 1997; Molnar et al., 1998; Super et al., 1998; Super and Uylings, 2001; Sarnat and Flores-Sarnat, 2002; Xie et al., 2002; Hevner et al., 2003; Jacobs et al., 2007). The hypothesis that a permanent, catastrophic extermination of preplate neurons accounts for the targeted ablation must be rejected because the suppression of GPT neurons is transient (i.e. killed cells are replaced) and the apoptosis of GPT neurons is graded (i.e. killed cells are compounded additively by serial ganciclovir treatments during progenitor vulnerability).

The present study provides support for additional conclusions of biological significance by integration of the cellular origins, morphogenesis and population dynamics of normal and ablated GPT cells. These conclusions address persistent issues regarding the specificity of the targeted ablation and the regulated development of the principal preplate neurons.

Specific cell killing eliminates a major fraction of GPT neurons in ablated mice

Binary poisoning by HSV-TK/ganciclovir can yield specific killing of target cells that express HSV-TK during S-phase, and non-specific killing of adjacent cells that do not express HSV-TK (Mesnil and Yamasaki, 2000). GPT neurons are one of the principal specific targets for ablation, as demonstrated directly by the co-localization of apoptosis and GPT reporters. Despite the dissemination of cellular lesions and the progressive failure of target gene expression in dying cells, the extent of apoptotic GPT neurons can be determined from the preponderance of morphological evidence and key statistical observations of densities of viable GPT neurons and apoptotic cells in control and ablated mice during and shortly after ganciclovir exposure

Half the peak density of non-phagocytic cells killed during early-onset apoptosis is a predictable shortfall of GPT neurons due to the killing mechanism of the targeted ablation initiated during asymmetric cell division. The remaining half consists of specifically killed GPT neuroblasts. Consistent with these interpretations, the sum of 50% of the apoptotic cell density and the total GPT neuron density observed on E13 shortly after ganciclovir treatment in the main group of ablated mice predictably and nearly attains the peak density of GPT neurons in littermate control mice, with similar results obtained throughout the first phase of apoptosis. Furthermore, the fraction of GPT neurons that escapes specific killing at E11–E12 is predictable from durations of effective ganciclovir action (5 h), S-phase (5 h), cell cycle (10 h) and intertreatment interval (12 h) (Kauffman, 1968; Takahashi et al., 1996). The observed survival of 11% in the main group of ablated mice matches the predicted survival of 10% for surviving GPT neurons generated during the E11–E12 period of the targeted ablation.

Based on this evidence, we conclude that the conditions tested in the present study specifically eliminate up to 90% of the normal complement of GPT neurons. Using the schedule of origin of BrdU-labelled GPT neurons in control mice, these methods can be extended to estimate the dose-dependency of specific cell killing in ancillary ablation groups. For example, three ganciclovir injections at E11–E12 eliminate up to 70%, two ganciclovir injections on E11 eliminate up to 36% and one ganciclovir injection on E11 eliminates up to 18% of the original unablated complement of GPT neurons. Qualitative observations of the magnitude of the defective neocortical phenotype of ablated mice match this ordered sequence.

Non-specific cell killing is insignificant, but structurally distinctive, in ablated mice

HSV-TK/ganciclovir ablations are often associated with non-specific 'bystander' killing, an apoptotic amplification by three possible mechanisms: intercellular toxin transfer via gap junctions, intercellular toxin transfer by endocytosis and/or local immunological activation by extracellular toxin. The extent of bystander killing in the predominant unscarred dorsal pallium can be determined with reasonable certainty by key statistical observations of ratios of apoptotic cell densities in ablated mice to GPT neuron densities in control mice during and shortly after ganciclovir exposure.

Excess dying cells in ablated mice accumulate after the rapid saturation of clearance mechanisms (Thomaidou et al., 1997). High ratios of dying to normal cells would reveal amplification, particularly via gap junctions, with a range of predicted values between 6:1 (oncological studies) and 100:1 (dye-coupling of neuronal progenitors) (LoTurco and Kriegstein, 1991; Nadarajah et al., 1997; Mesnil and Yamasaki, 2000; Bahrey and Moody, 2003). The observed ratio at E13 is 2:1 (131×10^3 cells/mm^3:63×10^3 neurons/mm^3), a value incongruent with apoptotic amplification, but consistent with the specific killing of either symmetrically divided pairs of GPT neurons derived from a GPT progenitor, or asymmetrically divided pairs of GPT neurons and GPT neuroblasts derived from a GPT progenitor. The characteristic reorganization of the proliferative matrix in the ventricular zone and the proliferative replacement of GPT neurons in ablated mice are in accordance with only the latter condition. Based on this evidence, and comparable results throughout the first phase of apoptosis, we conclude that bystander killing plays an insignificant role in the unscarred neocortex of ablated mice.

The products of non-specific killing deserve close attention for their probative value, as well as for their required inclusion in a comprehensive survey of the impact of targeted ablation. Based on evidence presented by these distinct forms of cellular damage, we conclude that the specificity of the targeted ablation method, while not absolute, is sufficient to permit meaningful developmental analyses. Only one early form of non-specific killing can be recognized in the unscarred dorsal pallium of all ablated mice: dying macrophages, which ingest toxin by endocytosis from specifically killed neurons. A second early form of bystander killing is seen in scars, which are neither necessary nor sufficient to account for the unscarred ablation phenotype. Scars provide an alternative outcome where both GPT and non-GPT cells are clearly subject to ganciclovir-initiated apoptosis. These scars have two key features. First, they are limited in extent, unlike the widespread neuroepithelial collapse produced by early ionizing radiation (Bayer and Altman, 1991). Secondly, their location is restricted to the dorsomedial peak of the dorsal pallium, a site that divides capillary beds from anterior and middle cerebral arteries. This site is unvascularized in mice until E15, although capillaries penetrate all other dorsal pallial ventricular zones on E11 (Conradi and Sourander, 1980; Marin-Padilla, 1985). Here, serial ganciclovir treatments and slow toxin clearance may promote non-specific bystander killing due to inherent vascular defects that resemble those found in neoplastic tumours, the most intensely studied tissue model for bystander killing. Scars encompass killing of all available cell types, which suggests mediation by toxin endocytosis. Neuroepithelial collapse within the scars releases toxins into the ventricular CSF (cerebrospinal fluid). Endocytosis of toxin-contaminated

CSF from residual processes at the ventricular lumen or 'leaky' non-ciliated tanycytes may then non-specifically kill neurons in circumventricular organs. Hydrocephalus may originate later from the inherent structural weakness and impaired vascular drainage of the scars, a progressive organic effect often found in association with neoplastic forebrain tumours.

Replacement GPT neurons proliferate from GPT neuroblasts in ablated mice

The capacity for near-normal replacement of the complement of GPT neurons in ablated mice is unexpected and may shed light on the difficult problem of control of proliferation during neocortical development (Price and Willshaw, 2000). The key observation is the expression of HSV-TK in both GPT neuroblasts and neurons, a finding inferred, but not demonstrated, in our previous study (Xie et al., 2002), and congruent with molecular biological indicators of GPT expression (Landry et al., 1998). These asymmetrically divided progeny show a very early localization of the reporter-target for ganciclovir action during a shared S-phase within their common GPT progenitors, conditions required for apoptotic induction, but not coincident in ganciclovir-insensitive, G_0-phase (post-mitotic) GPT neurons or non-GPT cells (Moolten, 1986).

GPT neuroblasts are located entirely in the ventricular zone of the dorsal pallium for a short developmental period in normal and ablated mice. The occurrence and extent of addition of GPT neurons is determined by preceding levels of proliferation of GPT neuroblasts in these restricted sites. Newborn GPT neurons migrate radially to settle into the mantle and marginal zones, where they can be detected by less efficient τ-eGFP and lacZ reporters. The origin, migration and settlement patterns of GPT cells shown by HSV-TK match the morphological trail of apoptotic cells in ablated mice. Also, birthdays of apoptotic cells and GPT neurons in ablated mice fit these patterns when lacZ expression is corrected to the earlier, more accurate, timing of HSV-TK expression. Finally, replacement of GPT neuroblasts and neurons fails only where the instructive artefact of neuroepithelial collapse of a ventricular zone scar in the dorsal pallium extirpates the proliferative source and radial migratory framework for newly generated cells.

Based on this evidence, we conclude that, like normal GPT neurons, replacement GPT neurons in ablated mice arise entirely by extended *de novo* proliferation from GPT neuroblasts. Regulation, modulation and technical sensitivity may contribute to differences in reporter efficiency, but *de novo* expression and/or up-regulation of GPT in post-mitotic neurons that normally do not localize GPT are neither apparent nor consistent with the data, unlike trophic determinations of transmitter identity in sympathetic ganglion neurons (Patterson, 1978).

Replacement GPT neuroblasts originate from non-GPT progenitors in ablated mice

GPT neuroblasts first arise from non-GPT progenitors, then self-replicate for a limited period by asymmetric division as shown by HSV-TK expression in unablated experimental mice. Self-replication of GPT neuroblasts is largely eliminated by specific cell killing during the period of ganciclovir-induced apoptosis in ablated mice, when neocortical development falters, but does not fail. Simultaneously, dying GPT neurons are accumulated in an additive, continuous fashion. The key observations are the reconstitution and extended replacement of GPT neuroblasts during and shortly after their targeted ablation, which uncover a mechanism of proliferative plasticity for the subsequent replacement of killed GPT neurons.

Based on this evidence, we conclude that, like the initial pool of normal GPT neuroblasts, a substantial component of replacement GPT neuroblasts seen during ganciclovir treatment in ablated mice originate and replenish by proliferation from prior progenitors. These progenitors are invulnerable to ganciclovir-induced ablation due to lack of GPT expression, and neither do they seem to be prone to bystander killing from dying GPT cells within the ablated ventricular zone. This progenitor–neuroblast–neuron lineage sequence identifies the GPT neuroblasts as intermediate progenitor cells. Their programmed death after three to five cycles of asymmetric division would account, at least in part, for the regulated accumulation of viable GPT neurons and the early high levels of apoptosis normally encountered in the ventricular zone of the dorsal pallium. The lineage sequence appears to be obligatory and unidirectional, with no apparent bypass towards cortical plate instead of preplate assembly or reversal from cortical plate to preplate assembly.

Such lineage sequences contribute to the amplification, regulation and diversification of cell division in neocortex (Kriegstein et al., 2004; Pontious et al., 2008). The best known example occurs in the late generation of the subventricular zone and supragranular neurons (Noctor et al., 2001). The new data indicate that a comparable sequence may also be employed in the ventricular zone by early neuronal progenitors. The harnessing of HSV-TK/ganciclovir ablation to GPT expression is a significant technical improvement for studies of intact brain because, unlike previous ablative agents such as ionizing radiation or the anti-mitotic methylazoxymethanol (Bayer and Altman, 1991; Cattabeni and DiLuca, 1997), the new attack spares prior progenitors, specifically kills intermediate progenitors of GPT neurons and largely saves the proliferative matrix of the ventricular zone from neuroepithelial collapse.

The complement of GPT neurons is inductively regulated in ablated mice

Ablated and normal mice eventually attain similar peak total complements of viable GPT neurons. A key observation is obtained from ablated mice, which display a proliferative capacity to replenish and replace killed cells by generating nearly twice the total complement of GPT neurons found in normal mice, with no alteration of the cell-cycle duration among GPT neuroblasts. Based on this evidence, we conclude

that the total complement of viable GPT neurons in ablated mice is inductively regulated by the fates of their cell lineage predecessors (Edelman, 1988). This regulation, also embedded in control mice, involves both positive and negative feedback, since substantial shortfalls or excesses of the total population of viable GPT neurons are avoided. The regulation appears to be global for the dorsal pallium, which may reflect numerous local cellular interactions widely distributed throughout its proliferative ventricular zone. Despite previous speculation (Noebels et al., 1991; Johnson, 1993; Chenn and McConnell, 1995; Sestan et al., 1999), its mechanisms are presently uncharted.

It is important to recall that neocortical growth is abridged in ablated mice, which leads to excessive, transient local accumulations of viable GPT neurons. The scale of this supranormal local replacement of GPT cells is paradoxical with regard to ganciclovir-induced reductions of mitotic activity immediately adjacent to the ventricle in the dorsal pallium of ablated mice. However, ablative harrowing of the proliferative matrix of the ventricular zone evokes its structural reorganization. The periventricular mitotic array converts from a flat, thin configuration into a perforated, thick configuration, which expands the vertical complement of mitotic progenitors, enlarges regenerative capacity and apparently restricts horizontal growth. This structural accommodation could disrupt progenitor fluidity within the proliferative matrix and misdirect radial migration unless locally corrected (Rakic, 1988; Walsh and Cepko, 1993). Ganciclovir-induced apoptosis is accompanied by a transient shift in the dominant cleavage plane of mitotic cells in the dorsal pallial ventricular zone, which may contribute to the early replacement of GPT neuroblasts in ablated mice by the symmetric division of their non-GPT progenitors (Sanada and Tsai, 2005). However, this shift may also reflect a dissociation of cellular cleavage and division planes (Konno et al., 2008) that subserves a compensatory modification of radial migration. Dying GPT neurons in ablated mice enter an impaired migratory framework within a regenerating neuroepithelial matrix (Xie et al., 2002). The vertical cleavage plane may derail them from the outward-bound track of radial migration, confine them to the malleable ventricular zone and benefit the laminar assembly of ablated neocortex by sparing the marginal and mantle zones from the clearance of excessive killed cells.

Delayed preplate formation blocks projection axons from GPT neurons in ablated mice

A second unexpected finding is that GPT neurons in ablated mice conserve all of the definitive morphogenetic properties of the principal prelate neurons except one: they emit few pioneer projection axons, which consist mainly of corticothalamic fibres in normal mice (Jacobs et al., 2007). Sparse residual projections arise from GPT neurons generated before ganciclovir treatment, whereas surviving and replacement GPT neurons retain the capacity to emit local infracortical axons. Preplate formation is delayed in ablated mice due to replacement of killed GPT neurons. By inference, we conclude that this delayed settlement is an unavoidable timing error that desynchronizes the development of neocortex and thalamus, and arrests the outgrowth of axonal projections by GPT neurons. The mechanism underlying projection blockade is uncertain, but this outcome has significant implications for the 'handshake hypothesis' often used to explain the midcourse contact and subsequent guidance to cellular targets of developing, reciprocal corticothalamic and thalamocortical projections (Lopez-Bendito and Molnar, 2003). The primary defect of ablated mice is restricted to the principal preplate neurons, unlike *Tbr1*and *Pax6* mutants (Stoykova and Gruss, 1994; Hevner et al., 2002). The principal preplate neurons in ablated mice do not emit substantial, albeit unstable, projections that approach the pallial-subpallial boundary, unlike *Coup-tfi* mutants (Zhou et al., 1999). Thus ablated mice provide a novel opportunity to dissect apart the elements of the 'handshake hypothesis' because preplate neurons, a distal target for thalamocortical axons, are restored at an excessive local density, whereas preplate projections, a proximal target for thalamocortical axons, are never established.

The middle and deep laminae of the principal preplate neurons in control mice are well-situated to guide ingrowth of 'specific' thalamocortical axons for termination in neuropil arcades at the superficial and deep borders of infragranular pyramidal neurons in sensory neocortex (Molnar and Blakemore, 1995; Adams et al., 1997; Molnar et al., 1998). Both afferents and arcades are grossly diminished in ablated mice, which contribute to the dyslaminated appearance of neocortex despite the conserved laminar organization of its neuronal cell bodies. It is reasonable to speculate that inadequate thalamocortical connections, as well as their lack of pioneer corticothalamic projection axons, accelerate the diffuse, late-onset apoptosis of GPT neurons (Cowan et al., 1984), whereas spared infracortical connections are sufficient to support the survival of many non-GPT pyramidal neurons. These surviving neurons do not generate significant seizure activity in ablated mice, perhaps because of their isolation within an impaired neocortex that is, in turn, isolated from the rest of the brain.

ACKNOWLEDGEMENTS

We thank Professor Anthony Campagnoni for the transgenic mice used in the present study. Technical support was provided by Celia Campagnoni, Vance Handley, Yan Hong-Hu, Vilma Schonnman and Kathy Kampf. Dr Nick Brecha, Dr Carlos Cepeda, Dr Richard Sutton, Dr James Waschek and Ms Tracey Weir provided advice on the manuscript.

FUNDING

This work was supported by the National Institutes of Health [grant numbers NS33091, NS23022].

REFERENCES

Adams NC, Lozsadi DA, Guillery RW (1997) Complexities in the thalamocortical and corticothalamic pathways. Eur J Neurosci 9:204–209.

Allendoerfer KL, Shatz CJ (1994) The subplate, a transient neocortical structure: its role in the development of connections between thalamus and cortex. Ann Rev Neurosci 17:185–218.

Bahrey HLP, Moody WJ (2003) Voltage-gated currents, dye and electrical coupling in the embryonic mouse neocortex. Cerebral Cortex 13:239–251.

Bayer SA, Altman J (1990) Development of layer I and the subplate in the rat neocortex. Exp Neurol 107:48–62.

Bayer SA, Altman J (1991) Neocortical development. New York: Raven Press.

Bielle F, Griveau A, Narboux-Neme N, Vigneau S, Sigrist M, Arber S, Wassef M, Pierani A (2005) Multiple origins of Cajal-Retzius cells at the borders of the developing pallium Nat Neurosci 8:1002–1012.

Bush TG, Savidge TC, Freeman TC, Cox HJ, Campbell EA, Mucke L, Johnson MH, Sofroniew MW (1998) Fulminant jejuno-ileitis following ablation of enteric glia in adult transgenic mice. Cell 93:189–201.

Cattabeni F, DiLuca M (1997) Developmental models of brain dysfunctions induced by targeted cellular ablations with methylazoxymethanol. Physiol Rev 77:199–215.

Chenn A, McConnell SK (1995) Cleavage orientation and the asymmetric inheritance of Notch 1 immunoreactivity in mammalian neurogenesis. Cell 82:631–641.

Conradi NG, Sourander P (1980) The early internal vascularization of the rat brain. Morphological studies on fetuses of normal and protein-deprived mothers. Acta Neuropathol 50:131–138.

Cowan WM, Fawcett JW, O'Leary DD, Stanfield B (1984) Regressive events in neurogenesis. Science 225:1258–1265.

Del Rio JA, Heimrich B, Borrell V, Forster E, Drakew A, Alcantara S, Nakajima K, Miyata T, Ogawa M, Mikoshiba K, Derer P, Frotscher M, Soriano E (1997) A role for Cajal–Retzius cells and reelin in the development of hippocampal connections. Nature 385:70–74.

D'Herde K, Mussche S, Roberg K (2003) Morphological changes in dying cells. In: Cell Proliferation and Apoptosis (Hughes D, Mehmet H, eds), Oxford: BIOS Scientific Publishers.

Edelman GM (1988) Topobiology. New York: Basic Books.

Ghosh A, Shatz CJ (1993) A role for subplate neurons in the patterning of connections from thalamus to neocortex. Development 117:1031–1047.

Guillery, RW (2002) On counting and counting errors. J Comp Neurol 447: 1–7.

Hasling TA, Gierdalski M, Jablonska B, Juliano SL (2003) A radicalization factor in normal cortical plate restores disorganized radial glia and disrupted migration in a model of cortical dysplasia. Eur J Neurosci 17:467–480.

Haydar T, Ang E, Rakic P (2003) Mitotic spindle rotation and the mode of cell division in yhr developing telencephalon. Proc Natl Acad Sci USA 100:2890–2895.

Hevner R, Zecevic N (2006) Pioneer neurons and interneurons in the developing subplate. Philos Trans R Soc Lond B Biol Sci 361: 1477–1497.

Hevner RF, Miyashita-Lin E, Rubenstein JL (2002) Cortical and thalamic axon pathfinding defects in *Tbri1, Gbx2*, and *Pax6* mutant mice: evidence that cortical and thalamic axons interact and guide each other. J Comp Neurol 447:8–17.

Hevner RF, Neogi T, Englund C, Daza RA, Fink A (2003) Cajal–Retzius cells in the mouse: transcription factors, neurotransmitters, and birthdays suggest a pallial origin. Dev Brain Res 141:39–53.

Jacobs E, Campagnoni C, Kampf K, Reyes SD, Kalra V, Handley V, Xie R, Hong-Hu Y, Spreur V, Fisher RS, Campagnoni, AT (2007) Visualization of corticofugal projections during early cortical development in a τ-GFP-transgenic mouse. Eur J Neurosci 25:17–30.

Johnson AR (1993). Contact inhibition in the failure of mammalian CNS axonal regeneration. BioEssays 15:807–813.

Kauffman SL (1968) Lengthening of the generation cycle during embryonic differentiation of the mouse neural tube. Exp Cell Res 49:420–424.

Konno D, Shioi G, Shitamukai A, Mori A, Kiyonari H, Miyata T, Matsuzaki F (2008) Neuroepithelial progenitors undergo LGN-dependent planar divisions to maintain self-renewability during mammalian neurogenesis. Nat Cell Biol 10:93–101.

Kriegstein AR, Castaneda-Castellanos DR, Noctor SC (2004) Patterns of cortical neurogenesis. Clin Neurosci Res 4:2–8.

Landry CF, Pribyl TM, Ellison JA, Givogri MI, Kampf K, Campagnoni CW, Campagnoni AT (1998) Embryonic expression of the MBP gene: identification of a promoter region that targets transgene expression to pioneer neurons. J Neurosci 18:7315–7327.

Lopez-Bendito G, Molnar Z (2003) Thalamocortical development: how are we going to get there? Nat Rev Neurosci 4:276–289.

LoTurco JJ, Kriegstein AR (1991) Clusters of coupled neuroblasts in embryonic neocortex. Science 252:563–566.

Luskin MB, Shatz CJ (1985) Studies of the earliest generated cells of the cat's visual cortex: cogeneration of subplate and marginal zones. J Neurosci 5:1062–1075.

Marin-Padilla M (1971) Early prenatal ontogenesis of the cerebral cortex (neocortex) of the cat (*Felis domestica*). A Golgi study. I. The primordial neocortical organization. Z Anat Entwickl-Gesch 134:117–145.

Marin-Padilla M (1985) Early vascularization of the embryonic cerebral cortex: Golgi and electron microscopic studies. J Comp Neurol 241:237–249.

McConnell SK, Ghosh A, Shatz CJ (1994) Subplate pioneers and the formation of descending connections from cerebral cortex. J Neurosci 14:1892–1907.

Mesnil M, Yamasaki H (2000) Bystander effect in herpes simplex virus-thymidine kinase/ganciclovir cancer gene therapy: role of gap-junctional intercellular communication. Cancer Res 60:3989–3999.

Meyer G, Wahle P (1999) The paleocortical ventricle is the origin of reelin-expressing neurons in the marginal zone of the foetal human neocortex. Eur J Neurosci 11:3937–3944.

Molnar Z, Blakemore C (1995) How do thalamic axons find their way to the cortex? Trends Neurosci 18:389–397.

Molnar Z, Adams R, Blakemore C (1998) Mechanisms underlying the early establishment of thalamocortical connections in the rat. J Neurosci 18:5723–5745.

Moolten FL (1986) Tumour chemosensitivity conferred by inserted herpes thymidine kinase genes: paradigm for a prospective cancer control strategy. Cancer Res 46:5276–5281.

Nadarajah B, Jones AM, Evans WH, Parnavelas JG (1997) Differential expression of connexins during neocortical development and neuronal circuit formation. J Neurosci 17:3096–3111.

Noctor SC, Flint AC, Weissman TA, Dammerman RS, Kriegstein AR (2001) Neurons derived from radial glial cells establish radial units in neocortex. Nature 409:714–720.

Noebels JL, Marcom PK, Jalilian-Tehrani MH (1991) Sodium channel density in hypomyelinated brain increased by MBP gene deletion. Nature 352:431–434.

Ogawa M, Miyata T, Nakajima K, Yagyu K, Seike M, Ikenaka K, Yamamoto H, Mikoshiba K (1995) The reeler gene-associated antigen on Cajal–Retzius neurons is a crucial molecule for laminar organization of cortical neurons. Neuron 14:899–912.

Patterson PH (1978) Environmental determination of autonomic neurotransmitter functions. Ann Rev Neurosci 1:1–17.

Pontious A, Kowealczyk T, Englund C, Hevner RF (2008) Role of intermediate progenitor cells in cerebral cortex development. Dev Neurosci 30:24–32.

Price DJ, Willshaw DJ (2000) Mechanisms of Cortical Development. Oxford: Oxford University Press.

Rakic P (1988) Specification of cerebral cortical areas. Science 241:170–176.

Reep RL (2000) Cortical layer VII and persistent subplate cells in mammalian brains. Brain Behav Evol 56:212–234.

Robertson RT, Annis CM, Baratta J, Haraldson S, Ingeman J, Kageyama GH, Kimm E, Yu J (2000) Do subplate neurons comprise a transient population of cells in developing neocortex of rats? J Comp Neurol 426:632–650.

Sanada K, Tsai LH (2005) G proteins $\beta\gamma$ subunits and AGHS3 control spindle orientation and asymmetric cell fate of cerebral cortical progenitors. Cell 122:119–131.

Sarnat HB, Flores-Sarnat L (2002) Role of Cajal–Retziuz and subplate neurons in cerebral cortical development. Semin Pediatr Neurol 9:302–308.

Sestan N, Artavanis-Tsakonas S, Rakic P (1999) Contact-dependent inhibition of cortical neurite growth mediated by notch signaling. Science 286:741–746.

Sheppard AM, Pearlman AL (1997) Abnormal reorganization of preplate neurons and their associated extracellular matrix: an early manifestation of altered neocortical development in the reeler mutant mouse. J Comp Neurol 378:173–179.

Smart IHM (1973) Proliferative characteristics of the ependymal layer during the early development of the mouse neocortex: a pilot study based on recording the number, location and plane of cleavage of mitotic figures. J Anat 116:67–91.

Stoykova A, Gruss P (1994) Roles of Pax-genes in developing and adult brain as suggested by expression patterns. J Neurosci 14:1395–1412.
Super H, Uylings HB (2001) The early differentiation of the neocortex: a hypothesis on neocortical evolution. Cerebral Cortex 11:1101–1109.
Super H, Soriano E, Uylings HB (1998) The functions of the preplate in development and evolution of the neocortex and hippocampus. Brain Res Rev 27:40–64.
Takahashi T, Nowakowski RS, Caviness VS (1996) The leaving or Q fraction of the murine cerebral proliferative epithelium: a general model of neocortical neuronogenesis. J Neurosci 19:6183–6196.
Thomaidou D, Mione MC, Cavanagh JFR, Parnavelas JG (1997) Apoptosis and its relation to the cell cycle in the developing cerebral cortex. J Neurosci 17:1075–1085.
Valverde F, De Carlos JA, Lopez-Mascaraque L (1995) Time of origin and early fate of preplate cells in the cerebral cortex of the rat. Cerebral Cortex 5:483–493.
Van Cruchten S, Van den Broeck W (2002) Morphological and biochemical aspects of apoptosis, oncosis and necrosis. Anat Histol Embryol 31:214–223.
Verney C, Derer P (1995) Cajal–Retzius neurons in human cerebral cortex at midgestation show immunoreactivity for neurofilament and calcium-binding proteins. J Comp Neurol 359:144–153.
Walsh C, Cepko CL (1993) Clonal dispersion in proliferative layers of developing cerebral cortex. Nature 362:632–635.
Xie Y, Skinner E, Landry C, Handley V, Schonmann V, Jacobs E, Fisher RS, Campagnoni AT (2002) Influence of the embryonic preplate on the organization of the cerebral cortex: a targeted ablation model. J Neurosci 22:8981–8991.
Zecevic N, Rakic P (2001) Development of layer I neurons in the primate cerebral cortex. J Neurosci 21:5607–5619.
Zhou C, Qiu Y, Pereira FA, Crair MC, Tsai SY, Tsai MJ (1999) The nuclear orphan receptor COUP-TFI is required for differentiation of subplate neurons and guidance of thalamocortical axons. Neuron 24:847–859.

Received 14 July 2009/18 August 2009; accepted 26 August 2009
Published as Immediate Publication 7 October 2009, doi 10.1042/AN20090038